Inorg. Chem. **2003**, *42*, 2919–2932

Adjacent- versus Remote-Site Electron Injection in TiO_2 Surfaces Modified with Binuclear Ruthenium Complexes

Bobak Gholamkhass,[§] Kazuhide Koike,* Nobuaki Negishi, Hisao Hori, Taizo Sano, and Koji Takeuchi

Photoenergy Application Group, Institute for Environmental Management Technology, National Institute of Advanced Industrial Science and Technology (AIST), 16-1 Onogawa, Tsukuba West, Ibaraki 305-8569, Japan

Received February 4, 2003

Nanocrystalline thin films of TiO_2 cast on an optically transparent indium tin oxide glass were sensitized with ruthenium homo- and heterobinuclear complexes, $[LL'Ru(BL)RuLL']^{n+}$ ($n = 2, 3$), where L and L′ are 4,4′-dicarboxy-2,2′-bipyridine (dcb) and/or 2,2′-bipyridine (bpy) and BL is a rigid and linear heteroaromatic entity (tetrapyrido[3,2-*a*:2′,3′-*c*:3″,2″-*h*:2‴,3‴-*j*]phenazine (tpphz) or 1,4-bis([1,10]phenanthroline[5,6-*d*]imidazol-2-yl)benzene (bfimbz)). The photophysical behavior of the Ru(II)–Ru(II) diads in solution indicated the occurrence of intercomponent energy transfer from the upper-lying Ru → bpy charge-transfer (CT) excited state of the $Ru(bpy)_2$ moiety to the lower-lying Ru → dcb CT excited state of the Ru(bpy)(dcb) (or $Ru(dcb)_2$) subunit in the heterobinuclear complexes. These sensitizer diads adsorbed on nanostructured TiO_2 surfaces in a *perpendicular* or *parallel* attachment mode. Adsorption was through the dcb ligands on one or both chromophoric subunits. The behavior of the adsorbed species was studied by nanosecond time-resolved transient absorption and emission spectroscopy, as well as by photocurrent measurements. In the TiO_2-adsorbed samples where BL was bfimbz, the electron injection kinetics was very fast and could not be resolved because an electron is promoted from the metal center to the dcb ligand directly linked to the semiconductor. In the TiO_2-adsorbed samples where BL was tpphz, for which, in the excited state, a BL localization of the lowest-lying metal-to-ligand charge transfer (MLCT) is observed, slower injection rates (9.5×10^7 s^{-1} in $[(bpy)_2Ru(tpphz)Ru(bpy)(dcb^-)]^{3+}/TiO_2$ and 5.5×10^7 s^{-1} in $[(bpy)(dcb)Ru(tpphz)Ru(bpy)(dcb^-)]^{3+}/TiO_2$) were obtained. Among the systems, the heterotriad assembly $[(bpy)_2Ru(bfimbz)Ru(bpy)(dcb^{2-})]^{2+}/TiO_2$ gave the best photovoltaic performance. In the first case, this was attributed to a fast electron injection initiated from a dcb-localized MLCT; in the second case, this is attributed to improved molecular orientation on the surface, which was due to rigidity and, at the same time, linearity of the heterotriad system, resulting in a slower charge recombination between the injected electron and the hole.

Introduction

Nanocrystalline solar cells sensitized by ruthenium(II) polypyridine complexes, as alternatives to conventional solid-state photovoltaic devices, are presently under intense investigation.[1,2] Recently, the concept of using bi- or multinuclear metal complexes as new assemblies of molecular components, categorized as supramolecular systems,[3] has been introduced in an effort to achieve improved molecular

* Author to whom correspondence should be addressed. Fax: +81-29-861-8258. E-mail: k-koike@aist.go.jp.

§ Present address: Department of Chemistry, Graduate School of Science and Engineering, Tokyo Institute of Technology, Tokyo, Japan.

(1) (a) Desilvestro, J.; Grätzel, M.; Kavan, L.; Moser, J.; Augustynski, J. *J. Am. Chem. Soc*. **1985**, *107*, 2988. (b) O'Regan, B.; Grätzel, M. *Nature* **1991**, *353*, 737. (c) Amadelli, R.; Argazzi, R.; Bignozzi, C. A.; Scandola, F. *J. Am. Chem. Soc.* **1990**, *112*, 7099. (d) Argazzi, R.; Bignozzi, C. A.; Heimer, T. A.; Castellano, F. N.; Meyer, G. J. *J. Phys. Chem. B* **1997**, *101*, 2591. (e) Kamat, P. V. *Prog. Inorg. Chem*. **1996**, *44*, 273.

(2) (a) Huang, S. Y.; Schlichthorl, G.; Nozik, A.; Grätzel, M.; Frank, A. J. *J. Phys. Chem. B* **1997**, *101*, 2576. (b) Papageorgiou, P.; Barbé, C.; Grätzel, M. *J. Phys. Chem. B* **1998**, *102*, 4156. (c) Dloczik, L.; Ileperuma, O.; Lauermann, I.; Peter, L. M.; Ponomarev, E. A.; Redmond, G.; Shaw, N. J.; Uhlendorf, I. *J. Phys. Chem. B* **1997**, *101*, 10281. (d) Sayama, K.; Sugihara, H.; Arakawa, H. *Chem. Mater*. **1998**, *10*, 3825. (e) Nazeeruddin, Md. K.; Zakeeruddin, S. M.; Humphry-Baker, R.; Jirousek, M.; Liska, P.; Vlachopoulos, N.; Shklover, V.; Fischer, C.-H.; Grätzel, M. *Inorg. Chem*. **1999**, *38*, 6298.

(3) (a) *Comprehensive Supramolecular Photochemistry*; Atwood, J. L., MacNicol, D. D., Davies, J. E. D., Vögtle, F., Eds.; Pergamon/Elsevier: Oxford, 1996. (b) Steed, J. W.; Atwood, J. L. *Supramolecular Chemistry*; John Wiley & Sons: West Sussex, U.K., 2000. (c) Balzani, V.; Juris, A.; Venturi, M.; Campagna, S.; Serroni, S. *Chem. Rev*. **1996**, *96*, 759.

10.1021/ic0341237 CCC: $25.00
Published on Web 03/21/2003

Scheme 1

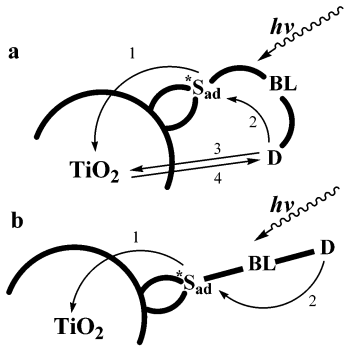

control of sensitizer orientation on the surface.[4] In these studies, flexible bridging ligands, 1,2-bis[4-(4′-methyl-2,2′-bipyridinyl)]ethane[4a] and 1,2-bis(4-pyridyl)ethane,[4b] have been employed to mediate between the donor and acceptor components of the supramolecular systems. In addition, by incorporating several chromophoric subunits into the structure of these supramolecular systems, one can increase the light-harvesting characteristic of the sensitizer throughout the visible region.[4c] The aim of these investigations is to produce a long-lived, photoinduced, charge-separated state by combining the intramolecular and interfacial electron-transfer processes.[5]

In an ideal case, following the photoexcitation of a sensitizer, S_{ad},[6] grafted to a semiconductor surface, TiO_2, a rapid interfacial electron injection occurs from the photosensitizer excited state, S_{ad}*, into the conduction band of the semiconductor (process 1 in Scheme 1). In this step, S_{ad} is an electron donor. Through a bridging ligand, BL, an intramolecular electron transfer from a covalently linked donor, D (hole scavenger), reduces the oxidized form of the sensitizer, S_{ad}^+ (process 2). In this step, S_{ad} is an electron acceptor. In certain cases, the intramolecular electron transfer may happen prior to electron injection, whereupon the reduced form of the sensitizer, S_{ad}^-, injects an electron into the conduction band.[4a] A reductant present in the contacting electrolyte can cause D^+ to revert to its normal state. All other rate-influencing parameters (such as redox potentials) being equal, the charge-separated state, $TiO_2(e^-)-S_{ad}-BL-D^+$, will live longer, because of the exponential decay of the electron-transfer rate with distance (in a simple diad system, the charge-separated state is $TiO_2(e^-)-S_{ad}^+$). The prolonged lifetime of the charge-separated state gives rise to an improved power output of the solar cell by lowering the quasi-Fermi level of the electrons in the semiconductor.[5] However, the flexibility of the bridging ligand allows a random geometry of the sensitizer on the nanocrystalline semiconductor surface and may provide a direct pathway for electron transfer and the succeeding charge recombination (see processes 3 and 4 in Scheme 1, panel a).[4c] Consequently, both a selective localization of the promoted electron in the excited state and the orientation of the dye molecules play crucial roles in achieving an efficient charge injection/separation.

Structurally, the present case can be explored by choosing $S_{ad}-BL-D$ systems in which the donor and the sensitizer are bound through a rigid and preferably linear BL (Scheme 1, panel b). In such a system, these chromophores, S_{ad} and D, can be fixed at a well-defined distance and orientation to increase the probability of obtaining a *heterotriad* system capable of performing useful tasks when anchored to the semiconductor surface.[1c,3,7]

To fulfill the previously described rigidity requirement, we synthesized a series of binuclear Ru(II)−Ru(II) complexes using the rigid and linear heteroaromatic entities tetrapyrido[3,2-*a*:2′,3′-*c*:3″,2″-*h*:2‴,3‴-*j*]phenazine[8] (tpphz) and 1,4-bis([1,10]phenanthroline[5,6-*d*]imidazol-2-yl)benzene[9] (bfimbz) as the BL. The former is a fully π-conjugated system exhibiting low-lying π*-orbitals,[8] whereas the latter could be considered as partially conjugated with a more elongated distance between the donor and the sensitizer. By employing these entities, in each case, we expect a selective localization of the promoted electron over the entire structure of the binuclear complexes, namely, on the BL in the tpphz complexes, and the remote ligands in the bfimbz ones. In addition, 4,4′-dicarboxy-2,2′-bipyridine (dcb), in which the interaction of carboxylic functional groups with the surface Ti ions is likely to lead to the formation of hydrogen or ester bonds (C−O−Ti),[10] and 2,2′-bipyridine (bpy) were used as nonbridging ligands. A combination of bpy and dcb on one

(4) (a) Kleverlaan, C. J.; Indelli, M. T.; Bignozzi, C. A.; Pavanin, L.; Scandola, F.; Hasselman, G. M.; Meyer, G. J. *J. Am. Chem. Soc*. **2000**, *122*, 2840. (b) Kleverlaan, C. J.; Alebbi, M.; Argazzi, R.; Bignozzi, C. A.; Hasselman, G. M.; Meyer, G. J. *Inorg. Chem.* **2000**, *39*, 1342. (c) Treadway, J. A.; Moss, J. A.; Meyer, T. J. *Inorg. Chem*. **1999**, *38*, 4386. (d) Argazzi, R.; Bignozzi, C. A.; Heimer, T. A.; Meyer, G. J. *Inorg. Chem.* **1997**, *36*, 2. (e) Nazeeruddin, M. K.; Humphry-Baker, R.; Grätzel, M.; Murrer, B. A. *Chem. Commun*. **1998**, 719.

(5) The power output, or simply the solar-cell voltage, is defined as the difference between the redox potential of the reductant, presented in the electrolyte, and the quasi-Fermi level of the electrons in the semiconductor. A maximum voltage can be obtained by fine-tuning these states, i.e., either lowering the Fermi level or raising the redox potential of the reductant. The electron concentration in the conduction band, which contributes in the determination of the quasi-Fermi level, can be enhanced by decreasing the electron escape flux against a constant electron injection one. This can be achieved by lengthening the lifetime of a charge-separated state in $TiO_2(e^-)-S_{ad}-BL-D^+$. See, for example: (a) Bonhôte, P.; Moser, J.-E.; Humphry-Baker, R.; Vlachopoulos, N.; Zakeeruddin, S. M.; Walder, L.; Grätzel, M. *J. Am. Chem. Soc*. **1999**, *121*, 1324. (b) Merrins, A.; Kleverlaan, C.; Will, G.; Rao, S. N.; Scandola, F.; Fitzmaurice, D. *J. Phys. Chem. B* **2001**, *105*, 2998. (c) Argazzi, R.; Bignozzi, C. A.; Heimer, T. A.; Castellano, F. N.; Meyer, G. J. *J. Am. Chem. Soc*. **1995**, *117*, 11815.

(6) Subscripts "a" and "d" are used to indicate that S acts as an electron donor in some processes and as an electron acceptor in other processes.

(7) See, for example: (a) Balzani, V.; Campagna, S.; Denti, G.; Juris, A.; Serroni, S.; Venturi, M. *Acc. Chem. Res*. **1998**, *31*, 26. (b) Prathapan, S.; Johnson, T. E.; Lindsey, J. S. *J. Am. Chem. Soc*. **1993**, *115*, 7519. (c) Gilat, S. L.; Kawai, S. H.; Lehn, J.-M. *J. Chem. Soc., Chem. Commun*. **1993**, 1439. (d) Credi, A.; Balzani, V.; Langford, S. J.; Stoddart, J. F. *J. Am. Chem. Soc*. **1997**, *119*, 2679. (e) Sauvage, J.-P.; Collin, J.-P.; Chambron, J.-C.; Guillerez, S.; Coudret, C.; Balzani, V.; Barigelletti, F.; De Cola, L.; Flamigni, L. *Chem. Rev*. **1994**, *94*, 993.

(8) (a) Bolger, J.; Gourdon, A.; Ishow, E.; Launay, J.-P. *Inorg. Chem*. **1996**, *35*, 2937. (b) Chiorboli, C.; Bignozzi, C. A.; Scandola, F.; Ishow, E.; Gourdon, A.; Launay, J.-P. *Inorg. Chem*. **1999**, *38*, 2402.

(9) Chao, H.; Ye, B.-H.; Zhang, Q.-L.; Ji, L.-N. *Inorg. Chem. Commun*. **1999**, *2*, 338.

(10) (a) Striplin, D. R.; Wall, C. G.; Erickson, B. W.; Meyer, T. J. *J. Phys. Chem. B* **1998**, *102*, 2383. (b) Nazeeruddin, M. K.; Kay, A.; Rodicio, I.; Humphry-Baker, R.; Muller, E.; Liska, P.; Vlachopoulos, N.; Grätzel, M. *J. Am. Chem. Soc.* **1993**, *115*, 6382. (c) Hou, Y.; Xe, P.; Zhang, B.; Cao, Y.; Xiao, X.; Wang, W. *Inorg. Chem.* **1999**, *38*, 6320.

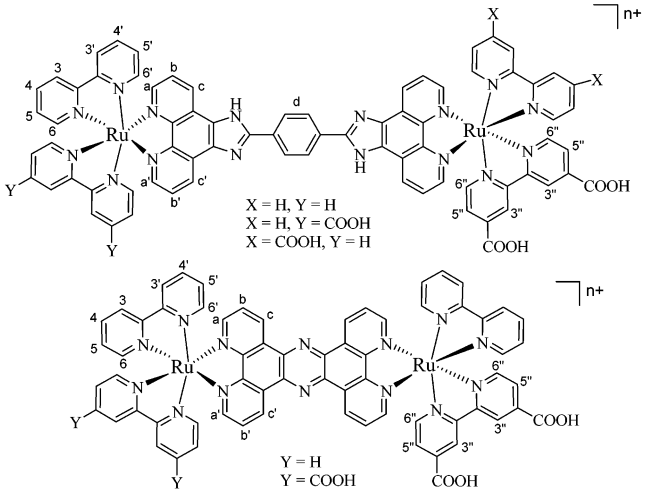

Figure 1. Structure and proton labeling of the homo- and heterobinuclear complexes synthesized in this work ($n = 3$ or 2, depending on the number of deprotonated carboxylic groups, *X* and *Y*).

or both chromophoric subunits of the binuclear complex allows a selective grafting of the dye sensitizer through one or two ends of the molecule. The present strategy also enabled us to improve the molecular orientation on the surface. The structures of the binuclear complexes synthesized in this work are illustrated in Figure 1.

Recently, a synthetic method for preparing a homobinuclear compound with bfimbz as the BL was reported.[9] However, because of the low solubility of the ligand in most solvents, this method cannot be used to prepare the mononuclear or heterobinuclear complexes.[11] The same is true for tpphz; reaction of the ligand with, for example, $Ru(bpy)_2Cl_2$ in ethylene glycol at high temperatures leads to the formation of homobinuclear complexes, because the mononuclear complexes are much more soluble than the free ligand.[8a] Therefore, a completely different synthetic strategy was applied in this work (see Synthesis under the Experimental Section).

Experimental Section

Instrumentation and Measurements. Absorption spectra were measured on a Hitachi model U-2001 spectrophotometer. Emission spectra were recorded with a Hitachi model F-3000 fluorescence spectrophotometer. These spectra were corrected for detector sensitivity, using *N*,*N*-dimethyl-*m*-nitroaniline, as described previously.[12] The dye solutions were bubble-degassed for 20 min with purified argon prior to the measurements. Emission lifetimes of the metal complexes were measured either with a Horiba model NAES-1100 time-correlated single-photon-counting system (the excitation source was a Horiba model NFL-111 nanosecond H_2 lamp, and the instrument response was <1 ns) or with a Continuum model YG680-10 Nd^{3+}:YAG pulse laser source (second-harmonic generation at 532 nm, 10-ns fwhm, 10 mJ/pulse). The fluorescence intensity was monitored with a Hamamatsu Photonics model R926 photomultiplier tube on a Jobin−Yvon model HR-320 monochromator. Time profiles of the fluorescence decays were stored with a Tektronix model SCD1000 digitizer (1-GHz bandwidth). Nanosecond laser spectroscopy was employed to measure the transient absorption spectra and corresponding lifetimes. The excitation-light source and light-correction optics were the same as those in the fluorescence lifetime measurement. An Ushio model 300-W Xe arc lamp was operated in a pulse-enhanced mode (500-μs duration) with an XC-300 power supply; a model YXP-300 light pulsar (Eagle Shoji Inc.) was used as the monitoring light source. Transient spectra were captured by a Princeton Instruments model IRY-700G/RB OMA detector head (700 channels; minimum gate width, 20 ns) on the HR-320 monochromator. The stored spectra were transferred to the computer via a Princeton Instruments model ST-100 OMA controller.

Electrospray ionization−mass spectroscopy (ESI-MS) was performed with a Hitachi model M1200H LC/MS system, using acetone as the eluant, unless described otherwise.

Redox potentials of metal complexes were measured by cyclic and differential-pulse voltammetry, using a BAS model 100B electrochemical analyzer in a standard three-cell electrode arrangement. Voltammograms were recorded using a platinum working electrode (diameter of 0.5 mm) in a solution of the complexes containing 0.1 mol of the supporting electrolyte, tetra-*n*-butylammonium hexafluorophosphate (TBAH), per liter of solution.

Materials. Acetonitrile (MeCN) was purified by fractional distillation from phosphorus oxide after having been dried for 1 day over 4 Å molecular sieves. All spectroscopic data were obtained on samples dissolved in the purified or spectral-grade solvents. Hydrated ruthenium trichloride was purchased from Kanto Chemical Co. and used as received. TBAH (Tokyo Kasei) was recrystallized from ethanol (EtOH). All other reagents were reagent-grade quality and were used without further purification.

Thin titania films on conducting indium tin oxide glass (10 Ω per square; Geomatic Co., Japan) were prepared by the thermal decomposition of titanium alkoxide deposited on the glass plates. The details of the procedure were reported previously.[12] The ruthenium compounds were coated onto the titania layer by dipping the glass plates for ∼12 h in a $10^{-5}-10^{-4}$ M solution of the complex in a 1:1 mixture of EtOH and MeCN at 50 °C.

Synthesis. 1,10-Phenanthroline-5,6-dione ($phenO_2$),[13] $[Ru(bpy)_2Cl_2]\cdot 2H_2O$,[14] $[(bpy)_2Ru(phenO_2)](PF_6)_2\cdot 2H_2O$,[15] $[Ru(DMSO)_4Cl_2]$, $[(bpy)Ru(DMSO)_2Cl_2]$,[16] $[(bpy)Ru(dcb)Cl_2]$, $[Ru(dcb)_2Cl_2]\cdot 2H_2O$,[17] tpphz, and $[(bpy)_2Ru(tpphz)](PF_6)_2\cdot 4H_2O$[8] were prepared according to the literature methods. The synthesis and purification methods used for the mononuclear and heterobinuclear complexes of bfimbz and tpphz are described below. All complexes were characterized by ^1H and, where needed, $^1H-^1H$ COSY NMR spectroscopy. For most of the complexes, the proton NMR signals were unambiguously assigned (see below).

(a) 4-([1,10]Phenanthroline[5,6-*d*]imidazol-2-yl)benzaldehyde (fimbzl). A portion (105 mg, 0.5 mmol) of $phenO_2$ in hot EtOH (20 mL) was added dropwise to a mixture of 335 mg (2.5 mmol) of terephthalaldehyde and 0.5 g of ammonium acetate in 50 mL of EtOH/water (4:1 mixture). A white precipitate formed within 5 min. The mixture was allowed to reflux for 3 h, and then was cooled and filtered. The crude product was washed with water and methanol (MeOH), dissolved in hot EtOH and reprecipitated by

(11) We use the prefix "hetero" to indicate an unsymmetrical arrangement of the remote ligands, bpy and dcb, around the Ru atoms in the binuclear complexes.

(12) Gholamkhass, B.; Koike, K.; Negishi, N.; Hori, H.; Takeuchi, K. *Inorg. Chem.* **2001**, *40*, 756.
(13) Amouyal, E.; Homsi, A.; Chambron, J.-C.; Sauvage, J.-P. *J. Chem. Soc., Dalton Trans.* **1990**, 1841.
(14) Sullivan, B. P.; Meyer, T. J. *Inorg. Chem.* **1978**, *17*, 3334.
(15) Goss, C. A.; Abruna, H. D. *Inorg. Chem.* **1985**, *24*, 4263.
(16) Evans, I. P.; Spencer, A.; Wilkinson, G. *J. Chem. Soc., Dalton Trans.* **1973**, 204.
(17) Zakeeruddin, S. M.; Nazeeruddin, M. K.; Humphry-Baker, R.; Grätzel, M.; Shklover, V. *Inorg. Chem.* **1998**, *37*, 5251.

the addition of water, filtered, washed with MeOH, and dried under vacuum. Yield: 53%, 85.3 mg. Further purification, in the case of 4-([1,10]phenanthroline[5,6-*d*]imidazol-2-yl)benzaldehyde (fimbzl), was performed on its metal complex, $[(bpy)_2Ru(fimbzl)](PF_6)_2$. (See section (c), $[(bpy)_2Ru(fimbzl)](PF_6)_2 \cdot 2H_2O$.)

(b) 1,4-Bis([1,10]phenanthroline[5,6-*d*]imidazol-2-yl)benzene (bfimbz). A vigorously stirred mixture of 33.5 mg (0.25 mmol) of terephthalaldehyde, 105 mg (0.5 mmol) of $phenO_2$, and 1.2 g of ammonium acetate in EtOH (100 mL) was refluxed for 7 h. During this time, the color gradually changed, because of the production of an orange precipitate. The reaction mixture was cooled, and EtOH was removed by rotary evaporation. After addition of water, the orange product was filtered off, washed with water and EtOH, and vacuum-dried. Yield: 79%, 101 mg. Anal. Calcd for $C_{32}H_{18}N_8$: C, 74.70; H, 3.53; N, 21.78. Found: C, 74.78; H, 3.72; N, 21.52.

(c) $[(bpy)_2Ru(fimbzl)](PF_6)_2 \cdot 2H_2O$. A mixture of $[Ru(bpy)_2Cl_2] \cdot 2H_2O$ (150 mg, 0.288 mmol) and fimbzl (85.3 mg, 0.263 mmol) in 50 mL of argon-purged EtOH/H_2O (4:1 mixture) was refluxed overnight. The solution was then cooled to room temperature and concentrated. A saturated solution of NH_4PF_6 in water was added to the concentrate. The orange precipitate was filtered off and washed with cold water. The product was subjected to column chromatography on an SP Sephadex C-25 column, using a 1:1 mixture of MeCN and an aqueous buffer (pH 4.1, containing 20 mM NH_4PF_6) as the eluant. A center cut of the orange band was collected. A saturated solution of NH_4PF_6 in H_2O was again added to the concentrate, and the precipitate was recrystallized from a MeOH/water mixture. Yield: 81%, 220 mg. Anal. Calcd for $C_{40}H_{28}F_{12}N_8OP_2Ru \cdot 2H_2O$: C, 45.12; H, 3.03; N, 10.53. Found: C, 44.92; H, 3.04; N, 10.82. ESI-MS *m*/*z*: 369, $[M - 2PF_6]^{2+}$; 737, $[M - 2PF_6 - H]^+$; 883, $[M - PF_6]^+$. ^1H NMR [CD_3CN] δ in ppm (integration, multiplicity), assignment: 12.51 (1H, b), NH; 10.12 (1H, d), CHO; 9.04 (1H, d), a′; 8.96 (1H, d), a; 8.53 (2H, d), 3′; 8.49 (2H, d), 3; 8.59 (1H, d), 8.46 (1H, d), 8.17 (1H, d) and 8.14 (1H, d), d (benzene ring protons); 8.13 (1H, dd), c′; 8.03 (1H, dd), c; 8.10 (2H, m), 4′; 7.98 (2H, m), 4; 7.86 (1H, dd), b′; 7.78 (1H, dd), b; 7.83 (2H, dd), 6′; 7.59 (2H, dd), 6; 7.45 (2H, multiple (m)), 5′; 7.21 (2H, m), 5. (See Supporting Information, Figure 1s.)

(d) $[(bpy)_2Ru(bfimbz)](PF_6)_2 \cdot 4H_2O$. A mixture of $[(bpy)_2Ru(fimbzl)](PF_6)_2$ (40 mg, 0.039 mmol), $phenO_2$ (12 mg, 0.057 mmol), and 0.5 g of ammonium acetate in argon-purged EtOH (30 mL) was refluxed for 5 h. The reaction mixture was cooled and concentrated by rotary evaporation. The concentrate was then cooled in an ice bath, and the orange precipitate that formed was filtered off, washed with water and EtOH, and vacuum-dried. The crude product was recrystallized from MeCN/EtOH. Yield: 53%, 26.5 mg. Anal. Calcd for $C_{52}H_{34}F_{12}N_{12}P_2Ru \cdot 4H_2O$: C, 48.42; H, 3.28; N, 13.03. Found: C, 48.19; H, 3.44; N, 12.75. ESI-MS *m*/*z*: 464, $[M - 2PF_6]^{2+}$; 927, $[M - 2PF_6 - H]^+$; 1073, $[M - PF_6]^+$. ^1H NMR [CD_3CN]: 11.85 (2H, (b)), NH; 8.88 (1H, b) a′; 8.67 (1H, b), a; 8.57 (4H, dd), 3 (3′); 8.52 (2H, dd), free end a (a′); 8.24 (2H, s) and 8.21 (2H, s), d; 8.12 (4H, dd), 4 (4′); 8.01 (4H, m), c (c′); 7.89 (4H, dd), 6 (6′); 7.62 (2H, dd), b (b′); 7.49 (4H, m), 5 (5′); 7.39 (1H, dd), free end b′; 7.33 (1H, dd), free end b.

(e) $[(bpy)_2Ru(bfimbz)Ru(bpy)(dcb^{2-})](PF_6)_2 \cdot 7H_2O$. $[(bpy)_2Ru(bfimbz)](PF_6)_2 \cdot 4H_2O$ (20 mg) and $[(bpy)Ru(dcb)Cl_2] \cdot 2H_2O$ (12 mg) were allowed to react in argon-purged ethylene glycol (5 mL) at 150 °C. After 1 h, the reaction mixture was cooled to room temperature, and the product was precipitated by the addition of an aqueous solution of NH_4PF_6 (10 mL). The orange precipitate was filtered off, washed with water, and recrystallized from a mixture of EtOH, MeOH, and a saturated solution of NH_4PF_6 in water. Yield: 70%, 20 mg. The product was further purified by column chromatography on an SP Sephadex C-25, using a 1:1 mixture of MeCN and an aqueous buffer (pH 6.8, containing 50 mM NH_4PF_6) as the eluant. Anal. Calcd for $C_{74}H_{48}F_{12}N_{16}O_4P_2Ru_2 \cdot 7H_2O$: C, 48.21; H, 3.39; N, 12.16. Found: C, 48.26; H, 3.42; N, 11.88. ESI-MS in MeOH/acetone (1:1) *m*/*z*: 357.5, $[M - 2PF_6 + 2H]^{4+}$; 476.3, $[M - 2PF_6 + H]^{3+}$; 714, $[M - 2PF_6]^{2+}$; 787, $[M - PF_6 + H]^{2+}$. ^1H NMR [CF_3COOD]: 9.43 (4H, d), a (a′); 8.83 (4H, s), d; 8.71−8.62 (8H, s, s and dd), 3 (3′, 3″); 8.45 (4H, d), c (c′); 8.34−8.16 (6H, m), 4 (4′); 8.14 (4H, m), b (b′); 8.05 (1H, d), 8.02 (3H, d), and 7.79 (4H, d), 6 (6′, 6″); 7.62 (4H, m), 7.46 (1H, t), and 7.42 (3H, t), 5 (5′, 5″).

(f) $[(bpy)(dcb)Ru(bfimbz)Ru(bpy)(dcb^-)](PF_6)_3 \cdot 5H_2O$. A mixture of 10 mg of bfimbz and 24 mg of $[(bpy)Ru(dcb)Cl_2] \cdot 2H_2O$ was heated at 170 °C in argon-purged ethylene glycol (5 mL). After 45 min, the reaction mixture was cooled to room temperature, and the product was precipitated by addition of an aqueous solution of NH_4PF_6 (10 mL). The orange precipitate was filtered off and washed with cold water. The crude product was dissolved in a 1:1 mixture of MeCN and aqueous buffer (pH 1.8) and subjected to column chromatography on an SP Sephadex C-25 column. A center cut of an orange-red band was collected by applying a 1:1 mixture of MeCN and an aqueous buffer (pH 5.0, containing 10 mM NH_4PF_6) as the eluant. The product was recrystallized by a slow evaporation of acetone from EtOH. Yield: 63%, 25 mg. Anal. Calcd for $C_{76}H_{49}F_{18}N_{16}O_8P_3Ru_2 \cdot 5H_2O$: C, 44.71; H, 2.91; N, 10.98. Found: C, 44.83; H, 3.11; N, 10.85. ESI-MS in MeOH/acetone (1:1) *m*/*z*: 379.5, $[M - 3PF_6 + H]^{4+}$; 505.6, $[M - 3PF_6]^{3+}$; 831, $[M - 2PF_6]^{2+}$. ^1H NMR [CF_3COOD]: 9.45 (4H, d), a (a′); 8.84 (4H, s), d; 8.69 (4H, s), 3″; 8.65−8.62 (4H, dd), 3 (3′); 8.44 (4H, d), c (c′); 8.25 (4H, m), 4 (4′); 8.13 (4H, m), b (b′); 8.01 (4H, d), 6″; 7.77 (4H, d), 6 (6′); 7.61 (4H, d), 5″; 7.40 (4H, m), 5 (5′).

(g) $[(bpy)_2Ru(tpphz)Ru(bpy)(dcb^-)](PF_6)_3 \cdot 4H_2O$. $[(bpy)_2Ru(tpphz)](PF_6)_2 \cdot 4H_2O$ (16.2 mg) and $[(bpy)Ru(dcb)Cl_2] \cdot 2H_2O$ (8.5 mg) were allowed to react in argon-purged ethylene glycol (5 mL) at 170 °C. After 10 min, the reaction mixture was cooled to room temperature, diluted with 10 mL of a 1:1 mixture of MeCN and an aqueous buffer (pH 1.8), and loaded onto an SP Sephadex C-25 column. A center cut of the orange band was collected by applying a 1:1 mixture of MeCN and an aqueous buffer (pH 5.0, containing 10 mM NH_4PF_6) as the eluant. Following the addition of saturated NH_4PF_6 to the concentrate, an orange precipitate formed. The product was filtered off, washed with water, and recrystallized by slow evaporation of acetone from EtOH. Yield: 52%, 13 mg. Anal. Calcd for $C_{66}H_{43}F_{18}N_{14}O_4P_3Ru_2 \cdot 4H_2O$: C, 43.91; H, 2.85; N, 10.86. Found: C, 44.02; H, 2.91; N, 10.77. ESI-MS in MeOH/acetone (1:1) *m*/*z*: 325, $[M - 3PF_6 + H]^{4+}$; 481.7, $[M - 2PF_6 + H]^{3+}$; 722, $[M - 2PF_6]^{2+}$; 795, $[M - PF_6 + H]^{2+}$. ^1H NMR [CD_3CN]: 9.94 (4H, dd), a (a′); 8.57 (2H, s), 3″; 8.54 (6H, dd), 3 (3′); 8.28 (4H, d), c (c′); 8.12 (4H, dd) and 8.05−8.01 (6H, m), overlapped 4 (4′) and b (b′); 7.86 (3H, d), 7.79 (1H, d), and 7.72 (4H, dd), 6 (6′, 6″); 7.48 (4H, m) and 7.25 (4H, m), 5 (5′, 5″). (See Supporting Information, Figure 1s.)

(h) $[(bpy)(dcb)Ru(tpphz)Ru(bpy)(dcb^-)](PF_6)_3 \cdot 6H_2O$. A mixture of 5 mg of tpphz and 14.2 mg of $[(bpy)Ru(dcb)Cl_2] \cdot 2H_2O$ was heated at 170 °C in argon-purged ethylene glycol (3 mL). After 2 h, the reaction mixture was cooled to room temperature, diluted with 7 mL of an aqueous buffer (pH 1.8) and MeCN (1:1), and loaded onto an SP Sephadex C-25 column. The main orange band was eluted with a 1:1 mixture of MeCN and an aqueous buffer (pH 4.5, containing 20 mM NH_4PF_6). Following the addition of saturated NH_4PF_6 to the concentrate, an orange precipitate formed. The product was filtered off, washed with cold water, and recrystallized from MeOH/MeCN/NH_4PF_6 (aq). Yield: 72%, 16.3

Scheme 2. Synthesis of Mono- and Binuclear Complexes Based on bfimbz.

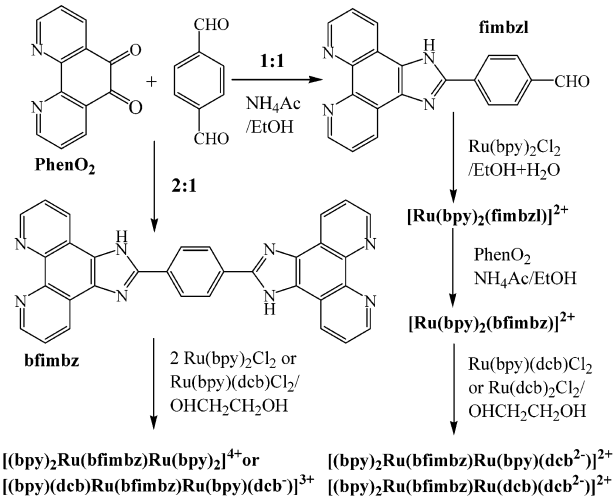

mg. Anal. Calcd for $C_{68}H_{43}F_{18}N_{14}O_8P_3Ru_2 \cdot 6H_2O$: C, 42.33; H, 2.87; N, 10.16. Found: C, 42.45; H, 2.89; N, 9.78. ESI-MS in MeOH/acetone (1:1) *m*/*z*: 347, $[M - 3PF_6 + H]^{4+}$; 511, $[M - 2PF_6 + H]^{3+}$; 839, $[M - PF_6 + H]^{2+}$. ^{1}H NMR [CD_3CN]: 9.94 (4H, m), a (a′); 8.58 (4H, s), 3″; 8.54 (4H, dd), 3 (3′); 8.28 (4H, dd), c (c′); 8.13 (4H, dd), 4 (4′); 8.01 (4H, m), b (b′); 7.86 (4H, d), 6″; 7.71 (4H, dd), 6 (6′); 7.48 (4H, m), 5″; 7.25 (4H, m), 5 (5′).

(i) $[(bpy)_2Ru(bfimbz)Ru(dcb)(dcb^{2-})](PF_6)_2 \cdot 5H_2O$. $[(bpy)_2Ru(bfimbz)](PF_6)_2 \cdot 4H_2O$ (12.5 mg) and $[Ru(dcb)_2Cl_2] \cdot 2H_2O$ (10 mg) were allowed to react in argon-purged ethylene glycol (3 mL) at 170 °C. After 1 h, the reaction mixture was cooled to room temperature, and a saturated aqueous solution of NH_4PF_6 was added to precipitate the complex. The reaction mixture was then centrifuged and decanted. The remaining orange precipitate was recrystallized from a MeOH/MeCN/H_2O mixture, filtered, and washed with cold water. Yield: 90%, 16.5 mg. Anal. Calcd for $C_{76}H_{48}F_{12}N_{16}O_8P_2Ru_2 \cdot 5H_2O$: C, 48.16; H, 3.08; N, 11.82. Found: C, 48.35; H, 3.15; N, 11.80. ^{1}H NMR [CF_3COOD]: 9.48 (4H, d), a (a′); 8.85 (4H, s), d; 8.71−8.62 (8H, m), 3 (3′, 3″); 8.47 (4H, d), c (c′); 8.26−8.10 (8H, m), overlapped 4 (4′) and b (b′); 8.04 (4H, d), 6″; 7.78 (4H, d), 6 (6′); 7.63 (4H, m), 5″; 7.42 (4H, m), 5 (5′).

Results and Discussion

Synthesis Route. Our synthesis strategy for the efficient preparation of the mononuclear complex $[(bpy)_2Ru(bfimbz)](PF_6)_2$ is presented in Scheme 2. In EtOH, the reaction of 1,10-phenanthroline-5,6-dione ($phenO_2$) with terephthalaldehyde in the presence of ammonium acetate (as a source of ammonia for imidazole ring closure) leads to the production of 4-([1,10]phenanthroline[5,6-*d*]imidazol-2-yl)benzaldehyde, fimbzl. This is the key step in the synthesis of the mononuclear building block $[(bpy)_2Ru(fimbzl)](PF_6)_2$ and the fully constructed $[(bpy)_2Ru(bfimbz)](PF_6)_2$, which can be prepared by another reaction between the aldehyde end of precoordinated fimbzl and $phenO_2$. In the following step, the second metallic moiety, $[(bpy)Ru(dcb)Cl_2]$ or $[Ru(dcb)_2Cl_2]$, is added to the free chelating site of the ligand. Therefore, only the desired heterobinuclear complexes, $[(bpy)_2Ru(bfimbz)Ru(bpy)(dcb^{2-})]^{2+}$ and $[(bpy)_2Ru(bfimbz)Ru(dcb^{2-})]^{2+}$, are obtained while homobinuclear byproducts are selectively avoided. Scrambling of the metallic moiety could still happen under the experimental conditions used for the synthesis, but the target heterobinuclear complexes can be isolated by column chromatography (see Experimental Section).

The ligand bfimbz can be obtained in a single step by reaction of 2 equiv of $phenO_2$ and 1 equiv of terephthalaldehyde. In ethylene glycol and at high temperatures (150−170 °C), the reaction of bfimbz with $[Ru(bpy)_2Cl_2]$ and $[(bpy)Ru(dcb)Cl_2]$ produced the homobinuclear complexes $[(bpy)_2Ru(bfimbz)Ru(bpy)_2]^{4+}$ and $[(bpy)(dcb)Ru(bfimbz)Ru(bpy)(dcb^-)]^{3+}$.

In the synthesis of the mononuclear building block based on tpphz, $[(bpy)_2Ru(tpphz)](PF_6)_2$ can be obtained by condensation of 5,6-diamino-1,10-phenanthroline with $phenO_2$ in $[(bpy)_2Ru(phenO_2)](PF_6)_2$.[8a] Similar to the reaction with bfimbz, direct reaction of 2 equiv of the metallic moiety with 1 equiv of tpphz leads to the homobinuclear complexes. With these choices of reaction partners, we obtained compounds with different numbers of bpy and dcb ligands in the desired positions of the supramolecular structure.

Electrochemical Properties. In all the compounds, the redox processes of the individual components were maintained in the supramolecular binuclear complexes. The half-wave potentials are presented in Table 1. The cyclic voltammograms of the complexes were consistent with a metal-based reversible oxidation and several ligand-based reductions. By analogy with $[Ru(bpy)_3]^{2+}$ and $[Ru(bpy)_2(dcb)]^{2+}$,[18] we assign the first reduction wave in the bfimbz complexes (at −1430 mV in dimethyl formamide (DMF) containing 0.1 M TBAH) to the dcb ligand.[19] This reduction potential is anodically shifted, with respect to that of $[Ru(bpy)_3]^{2+}$; the shift is due to the enhanced π-electron−acceptor characteristics of dcb. In $[(bpy)_2Ru(bfimbz)Ru(dcb)(dcb^{2-})](PF_6)_2$, the reduction wave (which was further shifted to −1350 mV) could be attributed to one of the dcb ligands.[19] However, for tpphz-containing binuclear complexes, the first reduction potential (−1200 mV) was equal to the first reduction potential of $[(bpy)_2Ru(tpphz)Ru(bpy)_2]^{4+}$. Launay et al. have shown that this binuclear complex is a significantly better electron acceptor than $[Ru(bpy)_3]^{2+}$, because of a low-lying lowest unoccupied molecular orbital (LUMO) mainly localized on the phenazine part of BL.[8] On the other hand, the reduction potentials of the

(18) Meyer, T. J.; Meyer, G. J.; Pfenning, B. W.; Schoonover, J. R.; Timpson, C. J.; Wall, J. F.; Kobusch, C.; Chen, X.; Peek, B. M.; Wall, C. G.; Ou, W.; Erickson, B. W.; Bignozzi, C. A. *Inorg. Chem.* **1994**, *33*, 3952.

(19) In $[(bpy)_2Ru(bfimbz)Ru(bpy)(dcb^{2-})](PF_6)_2$, the first reduction wave was observed at −1870 mV, exactly matching the second reduction potential of $[Ru(bpy)_3]^{2+}$. However, in a sample lot that precipitated from acidic media (0.1 M H_2SO_4) on addition of PF_6^-, the first reduction once again appeared at −1430 mV. Therefore, we conclude that either deprotonated dcb is not the active reduction site or the potential shift (from −1430 to −1870 mV) is a result of a diminished π-electron-acceptor ability in the anionic dcb. According to the present argument, the first reduction at −1425 mV in $[(bpy)(dcb)Ru(bfimbz)Ru(bpy)(dcb^-)](PF_6)_3$ can reasonably be attributed to the nonanionic dcb. In addition, the appearance of the first wave at −1350 mV in $[(bpy)_2Ru(bfimbz)Ru(dcb)(dcb^{2-})](PF_6)_2$, which is most probably due to the reduction of a nonanionic dcb, may indicate that, in this complex, the charge distribution is $[(bpy)_2Ru(bfimbz)Ru(dcb)(dcb^{2-})](PF_6)_2$ rather than $[(bpy)_2Ru(bfimbz)Ru(dcb^-)_2](PF_6)_2$.

Table 1. Redox Potentials of Ruthenium Complexes[a]

compound	redox potential (mV)	
	$E_{1/2}$ (ox)	$E_{1/2}$ (red)
$[Ru(bpy)_3]^{2+}$	+880	−1690, −1870, −2140
$[Ru(bpy)_3]^{2+}$[b]	+820	−1690, −1890, −1965, −2140
$[(bpy)_2Ru(BL_1)]^{2+}$	+930	−1770, −1990, −2180, −2325
$[(bpy)_2Ru(BL_1)]^{2+}$[b]	+815	−1685, −1825, −1965, −2195, −2465
$[(bpy)_2Ru(BL_1)Ru(bpy)_2]^{4+}$	+970	−1740
$[(bpy)_2Ru(BL_1)Ru(bpy)(dcb^{2-})]^{2+}$	+940−980[c]	−1430,[d] −1870, −1990, −2390
$[(bpy)(dcb)Ru(BL_1)Ru(bpy)(dcb^{-})]^{3+}$	+970	−1425,[d] −1820, −1950, −2330
$[(bpy)_2Ru(BL_2)Ru(bpy)(dcb^{-})]^{3+}$	+955, +1045	−1135, −1720, −2050, −2330
$[(bpy)_2Ru(BL_2)Ru(bpy)(dcb^{-})]^{3+}$[b]		−1210, −1855, −2035, −2180, −2430
$[(bpy)(dcb)Ru(BL_2)Ru(bpy)(dcb^{-})]^{3+}$	+950	−1130, −1365, −1760, −2100, −2400
$[(bpy)(dcb)Ru(BL_2)Ru(bpy)(dcb^{-})]^{3+}$[b]		−1195, −1425, −1615, −1825, −1965
$[(bpy)_2Ru(BL_1)Ru(dcb)(dcb^{2-})]^{2+}$		−1300, −1440, −1740, −1970, −2320
$[(bpy)_2Ru(BL_1)Ru(dcb)(dcb^{2-})]^{2+}$[b]	+940, +1190	−1350, −1795, −2000, −2390

[a] BL_1 represents bfimbz; BL_2 represents tpphz. The values were obtained at room temperature and in MeCN solutions containing 0.1 M TBAH. All $E_{1/2}$ values are referenced to the $E_{1/2}$ of the ferrocenium$^+$/ferrocene redox couple (380 mV vs SCE in MeCN); for comparison, the redox potentials of $[Ru(bpy)_3]^{2+}$ are also presented. [b] In DMF (0.1 M TBAH). [c] Not clearly resolved. [d] Observed only in samples that precipitated from acidic media.

Table 2. Spectroscopic and Photophysical Properties of the Ruthenium Complexes[a]

compound	λ_{abs}[b]/nm (ϵ_{max}[c]/10^3 M^{-1} cm^{-1})		λ_{em}[b]/nm		τ[d]/ns at	ϕ_{em}[e]
	$\pi-\pi^*$	MLCT	at 298 K	at 77 K	298 K	at 298 K
$[(bpy)_2Ru(BL_1)]^{2+}$	235 (53.8), 286 (93.1), 369 (49.6)	456 (19.6)	623	587	1250	0.115
$[(bpy)_2Ru(BL_1)Ru(bpy)_2]^{4+}$	241 (81.6), 286 (166.6), 354 (71.8)	460 (43.6)	625	589	1060	0.057
$[(bpy)_2Ru(BL_1)Ru(bpy)(dcb^{2-})]^{2+}$	243 (77.4), 286 (147.0)	461 (44.5)	630	615	240	
	352 (63.6)				1300	0.086
$[(bpy)(dcb)Ru(BL_1)Ru(bpy)(dcb^{-})]^{3+}$	244 (69.9), 287 (124.8), 355−369 (55.0)	454 (17.5)[f]	662	647	1170[g]	0.014
$[(bpy)_2Ru(BL_2)Ru(bpy)(dcb^{-})]^{3+}$	245 (71.9), 282 (183.2)	444 (41.5)	640	603	40	
	351 (33.4), 370 (40.0)				1000	0.0037
$[(bpy)(dcb)Ru(BL_2)Ru(bpy)(dcb^{-})]^{3+}$	244 (71.9), 282 (153.5), 352 (31.3), 370 (36.3)	446 (33.9)	655	627	670[g]	0.0067
$[(bpy)_2Ru(BL_1)Ru(dcb)(dcb^{2-})]^{2+}$[h]	242 (74.4), 287 (117.0)	459 (36.9)	650	624	40	
	355 (62.0)				1250	0.033

[a] BL_1 represents bfimbz; BL_2 represents tpphz. All the complexes are PF_6 salts. The values were obtained in MeCN at room temperature, unless otherwise noted. [b] Uncertainties in λ_{abs} and λ_{em} are ±1 and ±2 nm, respectively. The emission maximum at 77 K is taken in *n*-butyronitrile glass. [c] Estimated error in ϵ_{max} is ±5%. [d] Uncertainty in lifetime values is <6%. [e] Emission quantum yields, relative to $[Ru(bpy)_3]^{2+}$: $\phi_{em} = 0.061$. [f] The lowest MLCT band maximum. [g] In these homobinuclear complexes, a weak contribution from faster decays could be observed; however, the decay profiles become monotonic in samples precipitated from acidic media. [h] In MeCN/MeOH (4:1 in absorption measurements and 8:1 in emission measurements).

bfimbz mononuclear complex $[(bpy)_2Ru(bfimbz)](PF_6)_2$ were comparable to those of $[Ru(bpy)_3]^{2+}$, confirming the absence of a low-lying molecular orbital in bfimbz. In line with these results, and on the basis of the known correlation between the electrochemical and spectroscopic properties,[20,21] the lowest-lying metal-to-ligand charge-transfer (MLCT) state is expected to reside on the remote dcb ligand and not on the bfimbz BL. The case is reversed in the tpphz complexes; i.e., in the excited state, a BL localization of the lowest-lying MLCT state is expected.[8b]

For the metallic centers, oxidation waves occurred at potentials slightly more positive (+930 to +1190 mV in MeCN containing 0.1 M TBAH) than those of the Ru(III)/Ru(II) couple in $[Ru(bpy)_3]^{2+}$ (+880 mV), with $[(bpy)_2Ru(bfimbz)]^{2+}$ showing the smallest shift and the heterobinuclear $[(bpy)_2Ru(bfimbz)Ru(dcb)(dcb^{2-})]^{2+}$ showing the largest shift. This trend is commonly observed in complexes containing π-acceptor ligands such as dcb.[21] The increased differences on going from mono- to heterobinuclear complexes can also result from the presence of the second metal center, which is expected to cause some stabilization in the LUMO of the BL and, because of back-bonding, of the metal-centered highest occupied molecular orbital.[22] However, as anticipated, neither of the BLs allowed substantial electronic communication across the bridge; thus, the connected subunits maintained their intrinsic redox properties within the supramolecular structure.

Absorption and Luminescence Properties. (a) In Solution. Absorption and emission maxima, molar extinction coefficients, emission lifetimes, and quantum yields for all the complexes are gathered in Table 2. Absorption spectra of selected dissolved and TiO_2-adsorbed complexes are shown in Figure 2. Absorption features appearing in the visible region (400−550 nm) correspond to spin-allowed ^{1}MLCT transitions. The spectra exhibited by the binuclear complexes overlap with an almost doubled spectrum of the component unit $[(bpy)_2Ru(BL)](PF_6)_2$. Once again, this indicates that we are dealing with a class of binuclear

(20) (a) Meyer, T. J. *Pure Appl. Chem.* **1986**, *58*, 1193. (b) Juris, A.; Balzani, V.; Barigelletti, F.; Campagna, S.; Belser, P.; von Zelewsky, A. *Coord. Chem. Rev.* **1988**, *84*, 85. (c) Vlcek, A. A.; Dosdworth, E. S.; Pietro, W. J.; Lever, A. B. P. *Inorg. Chem.* **1995**, *34*, 1906. (d) Barigelletti, F.; Juris, A.; Balzani, V.; Belser, P.; von Zelewsky, A. *Inorg. Chem.* **1987**, *26*, 4115.

(21) Kalyanasundaram, K. *Photochemistry of Polypyridine and Porphyrin Complexes*; Academic Press: San Diego, CA, 1992.

(22) (a) Hammarström, L.; Barigelletti, F.; Flamigni, L.; Indelli, M. T.; Armaroli, N.; Calogero, G.; Guardigli, M.; Sour, A.; Collin, J.-P.; Sauvage, J.-P. *J. Phys. Chem. A* **1997**, *101*, 9061. (b) Collin, J.-P.; Lainé, P.; Launay, J.-P.; Sauvage, J.-P.; Sour, A. *J. Chem. Soc., Chem. Commun.* **1993**, 434.

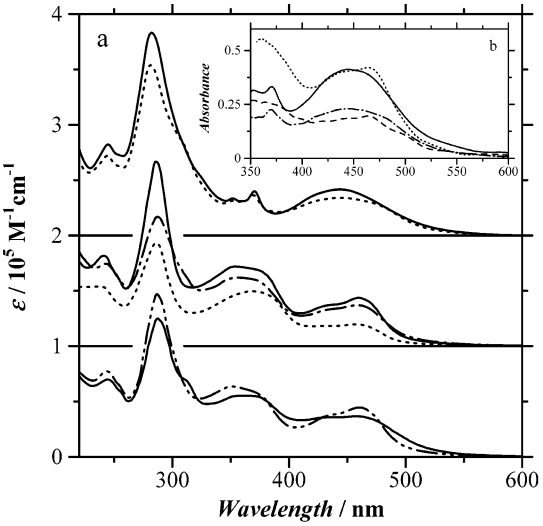

Figure 2. **(a)** Absorption spectra of $[(bpy)_2Ru(tpphz)Ru(bpy)(dcb^-)]^{3+}$ (solid line, upper panel), $[(bpy)(dcb)Ru(tpphz)Ru(bpy)(dcb^-)]^{3+}$ (dotted line, upper panel), $[(bpy)_2Ru(bfimbz)Ru(bpy)_2]^{4+}$ (solid line, middle panel), $[(bpy)_2Ru(bfimbz)Ru(dcb)(dcb^{2-})]^{2+}$ (dotted−dashed line, middle panel), $[(bpy)_2Ru(bfimbz)]^{2+}$ (dotted line, middle panel), $[(bpy)_2Ru(bfimbz)Ru(bpy)(dcb^{2-})]^{2+}$ (dot-dot−dashed line, lower panel), and $[(bpy)(dcb)Ru(bfimbz)Ru(bpy)(dcb^-)]^{3+}$ (solid line, lower panel) in MeCN solution. (b) Ground-state absorption spectra observed following the adsorption of the sensitizer dyes onto TiO_2: $[(bpy)_2Ru(bfimbz)Ru(dcb)(dcb^{2-})]^{2+}/TiO_2$ (dotted line), $[(bpy)_2Ru(tpphz)Ru(bpy)(dcb^-)]^{3+}/TiO_2$ (solid line), $[(bpy)(dcb)Ru(tpphz)Ru(bpy)(dcb^-)]^{3+}/TiO_2$ (dotted−dashed line), and $[(bpy)(dcb)Ru(bfimbz)Ru(bpy)(dcb^-)]^{3+}/TiO_2$ (dashed line). The absorption spectra of the adsorbed samples were obtained by subtracting the absorption of the bare TiO_2 films from that of the sensitized ones.

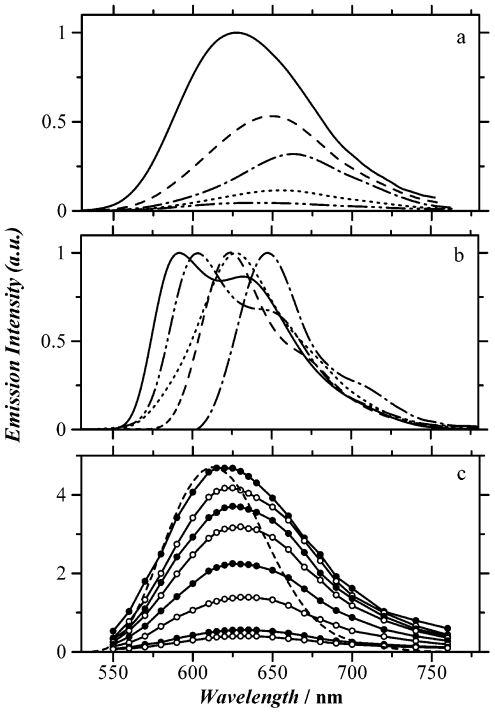

Figure 3. Corrected emission spectra of (—) $[(bpy)_2Ru(bfimbz)Ru(bpy)(dcb^{2-})]^{2+}$ in MeCN/MeOH (8:1) and (− − −) $[(bpy)_2Ru(bfimbz)Ru(dcb)(dcb^{2-})]^{2+}$, (− · −)$[(bpy)(dcb)Ru(bfimbz)Ru(bpy)(dcb^-)]^{3+}$, (- - -) $[(bpy)(dcb)Ru(tpphz)Ru(bpy)(dcb^-)]^{3+}$, and (−··−) $[(bpy)_2Ru(tpphz)Ru(bpy)(dcb^-)]^{3+}$ in MeCN (a) at room temperature and (b) in *n*-BuCN at 77 K. Panel c shows time-resolved emission spectra of $[(bpy)_2Ru(bfimbz)Ru(dcb)(dcb^{2-})]^{2+}$ in MeCN/MeOH (8:1) at 10 ns, 50 ns, 100 ns, 200 ns, 500 ns, 1 μs, 2 μs, and 2.4 μs. The dashed line is the steady-state (uncorrected) emission spectrum of the compound in MeCN/MeOH (8:1).

metal compounds with minimum electronic communication across the bridge.

The intense absorption band in the UV region (ca. 286 nm, $\epsilon > 10^5$ M^{-1} cm^{-1}) is due to ligand-centered transitions mainly associated with polypyridine units. Thus, the molar absorptivity scales as the total number of electronically decoupled bpy moieties present in the structure of the binuclear complexes. For the tpphz complexes, two sharp bands characteristic of the tpphz BL appear at 350 and 370 nm, corresponding to $\pi-\pi^*$ transitions. In the bfimbz complexes, a broad band in the 320−390 nm range can be assigned to the bfimbz BL. For this band, the observed maxima are at 370, 350, and 350 nm in $[(bpy)_2Ru(bfimbz)]^{2+}$, $[(bpy)_2Ru(bfimbz)Ru(bpy)_2]^{4+}$, and $[(bpy)_2Ru(bfimbz)Ru(bpy)(dcb^{2-})]^{2+}$, respectively. For most of the bfimbz binuclear complexes, this broad band seems to be asymmetrically deformed, which indicates contributions of new molecular orbital coefficients (to form this band) in the absorption spectra of binuclear complexes. In the mononuclear complex, it is most likely that the higher-energy side of this band originates from the bfimbz $\pi-\pi^*$ transitions perturbed by the presence of the metal center.

Figure 3 shows the corrected emission spectra. All the complexes exhibit the characteristic MLCT luminescence both in the rigid matrix at 77 K and in fluid solution at room temperature.[20b,23] This assignment is based on the fact that the emission spectra show a vibrational progression of 1200−1300 cm^{-1} at 77 K (Figure 3b), which is due to a bpy-localized mode.[24] In addition, the spectra are centered at shorter wavelengths than the ambient temperature spectra are. At room temperature (Figure 3a), however, the emission spectra are broad and structureless, possessing lifetimes (0.5−1.2 μs) very close to the lifetime of the MLCT excited state of $[Ru(bpy)_3]^{2+}$.[20a,21] In the heterobinuclear complexes, we observed a biphasic decay rate with a contribution from a shorter lifetime component (40−300 ns; see below).

On comparing the dcb-containing hetero- and homobinuclear complexes $[(bpy)_2Ru_A(BL)Ru_B(bpy)(dcb)]^{n+}$ (or $[(bpy)_2Ru_A(BL)Ru_B(dcb)_2]^{n+}$) and $[(bpy)(dcb)Ru(BL)Ru(bpy)(dcb)]^{n+}$ (n = 2 or 3), we found that, at room temperature, the emission band maxima of the homobinuclear complexes are shifted to lower energies. The similarity in the visible region of the excitation and absorption spectra of these complexes in MeCN demonstrates that an intercomponent energy transfer occurs from the upper-lying Ru → bpy CT excited state of the $Ru_A(bpy)_2$ moiety to the lower-lying Ru → dcb CT excited state of the $Ru_B(bpy)(dcb)$ (or $Ru_B(dcb)_2$) subunit of the heterobinuclear complex(es). Time-

(23) Kober, E. M.; Caspar, J. V.; Sullivan, B. P.; Meyer, T. J. *Inorg. Chem.* **1988**, *27*, 4587.

(24) (a) Caspar, J. V.; Meyer, T. J. *Inorg. Chem.* **1983**, *22*, 2444. (b) Kober, E. M.; Caspar, J. V.; Lumpkin, R. S.; Meyer, T. J. *J. Phys. Chem.* **1986**, *90*, 3722. (c) Barkawi, K. R.; Murtaza, Z.; Meyer, T. J. *J. Phys. Chem.* **1991**, *95*, 97. (d) Omberg, K. M.; Schoonover, J. R.; Treadway, J. A.; Leasure, R. M.; Dyer, R. B.; Meyer, T. J. *J. Am. Chem. Soc.* **1997**, *119*, 7013.

resolved emission spectroscopy, in the case of $[(bpy)_2Ru(bfimbz)Ru(dcb)(dcb^{2-})]^{2+}$ (Figure 3c), for example, revealed that early-time spectra are centered at shorter wavelengths, closely overlapping the steady-state emission spectra (here, the $\Delta\lambda_{max}$ difference of less than ± 7 nm can be ascribed to the systematic errors associated with the instruments used for measurement). The intercomponent energy-transfer rate, k_{en}, was monitored by comparing the ruthenium-based luminescence lifetime in the heterobinuclear complex (τ) with that of the reference complex $[(bpy)_2Ru(BL)]^{2+}$ (τ_0) (eq 1).

$$k_{en} = \frac{1}{\tau} - \frac{1}{\tau_0} \tag{1}$$

The values of k_{en} for $[(bpy)_2Ru(bfimbz)Ru(bpy)(dcb^{2-})]^{2+}$, $[(bpy)_2Ru(bfimbz)Ru(dcb)(dcb^{2-})]^{2+}$, and $[(bpy)_2Ru(tpphz)Ru(bpy)(dcb^{-})]^{3+}$ are 3.3×10^6, 8.2×10^6, and 2.4×10^7 s^{-1} (corresponding to respective driving forces of $\Delta G = -0.07$, -0.13, and -0.08 eV),[25] respectively. The difference in the k_{en} values of the two bfimbz-containing heterobinuclear complexes can be attributed to the driving force of the process, ΔG. In the tpphz-containing heterobinuclear complex, observation of a faster rate could be accounted for by the π-conjugation across the BL and a shorter donor−acceptor distance, leading to an eventual, stronger electronic interaction between the donor and acceptor subunits.

According to the aforementioned argument, the appearance of the emission band maximum at lower energies in the homobinuclear complexes $[(bpy)(dcb)Ru(BL)Ru(bpy)(dcb)]^{n+}$ can be well explained by the absence of a higher-lying and emissive Ru → bpy CT excited state originating from a would-be $Ru(bpy)_2$ moiety.

(b) Adsorbed on TiO_2. The TiO_2 films assumed a yellow color, because of adsorption of the dye. Following the sensitization, the adopted spectral features corresponded perfectly with those in solution within the observable window ($\lambda > 350$ nm).[26] In the TiO_2 films sensitized with binuclear complexes of tpphz, one of the two sharp bands is clearly observed at 370 nm. For all the adsorbed dyes, absorption maxima and the relative extinction coefficients at, for example, 370 and 450 nm resemble those in solution, which implies that the compound adsorbed to the TiO_2 surface with the same electronic distribution and geometry as the dissolved dye. Furthermore, in the complexes where there is only one dcb ligand in the structure of the sensitizing dye, namely, $[(bpy)_2Ru(bfimbz)Ru(bpy)(dcb^{2-})]^{2+}$ and $[(bpy)_2Ru(tpphz)Ru(bpy)(dcb^{-})]^{3+}$, the MLCT absorbance is doubled compared to those of the complexes with two dcb ligands, one on each metal (i.e., $[(bpy)(dcb)Ru(bfimbz)Ru(bpy)(dcb^{-})]^{3+}$ and $[(bpy)(dcb)Ru(tpphz)Ru(bpy)(dcb^{-})]^{3+}$, Figure 2b). This can be interpreted in terms of *perpendicular* versus *parallel* attachment of the dye molecules to the surface.[5] Assuming a surface with minimum defects, two perpendicularly attached dye molecules (one-site attachment mode) can be displaced instead of one parallel-grafted molecule (two-site attachment mode) if the dye molecules are adsorbed onto the surface through a certain number of carboxylic functional groups in a compact arrangement. Thus, it is obvious that the spectral observations directly originate from the rigidity of the BLs chosen for these systems. Moreover, we anticipate a high degree of occupancy of the semiconductor grafting sites. Attempts to synthesize a suitable mononuclear model compound were not successful, because of the low solubility of the mononuclear building blocks of $Ru(dcb)_2Cl_2$ and $Ru(dcb)(bpy)Cl_2$.

In addition to the mode of attachment (perpendicular versus parallel), another factor contributing to the surface occupancy is the relative horizontal and vertical surface coverage (HVSC) of the adsorbed molecules. The HVSC can be estimated from absorption ratios. For example, in the bfimbz system, a 2.1-fold increase in the absorption (at 460 nm) on going from $[(bpy)(dcb)Ru(bfimbz)Ru(bpy)(dcb^{-})]^{3+}/TiO_2$ to $[(bpy)_2Ru(bfimbz)Ru(bpy)(dcb^{2-})]^{2+}/TiO_2$ is a reasonable estimation for the HVSC in these binuclear complexes containing a long BL.[27] In the tpphz system, the HVSC is <1.8 (obtained from the absorption ratio of $[(bpy)_2Ru(tpphz)Ru(bpy)(dcb^{-})]^{3+}/TiO_2$ and $[(bpy)(dcb)Ru(tpphz)Ru(bpy)(dcb^{-})]^{3+}/TiO_2$ at 445 nm), because of the shorter BL, and the homobinuclear complex has a smaller horizontal surface coverage in a parallel attachment. In a perpendicular attachment, we expect the vertical surface coverages to be the same in both the bfimbz system $[(bpy)_2Ru(bfimbz)Ru(bpy)(dcb^{2-})]^{2+}$ and the tpphz system $[(bpy)_2Ru(tpphz)Ru(bpy)(dcb^{-})]^{3+}$.[27]

Assuming that the extinction coefficients for the adsorbed samples are similar to those in solution, we obtain experimental surface coverages of $\Gamma = (0.44-1.73) \times 10^{-7}$ mol cm^{-2}. These values are in the same range as those of closely related mononuclear ruthenium complexes reported in the literature.[28] It is worth noting that, regardless of whether a

(25) The driving force (± 0.02 eV) of the intercomponent energy transfer was calculated from the 0−0 band energy, E_{0-0}, of the emission spectra at 77 K, which itself is approximated to be larger than the maximum energy of the emission, E_{max}, by 200 cm^{-1}.

(26) The absorption spectra of the adsorbed samples were obtained by subtracting the absorption of the bare TiO_2 films from that of the sensitized films.

(27) (a) Assuming a value of 7.0 Å for the radius of $[(bpy)_2Ru(dcb)]^{2+}$ (from Trammell et al.[28]) and Ru−Ru distances of 20.7 Å in bfimbz systems (obtained by using CS ChemBats3D Pro, Version 5.0; CambridgeSoft Corp., Cambridge, MA, 1999) and 12.7 Å in tpphz systems,[8] we calculated a vertical surface coverage of 1.1×10^{-10} mol cm^{-2} for both systems in perpendicular attachments. Using a dumbbell shape for the structure of binuclear complexes, we calculated horizontal surface coverages of 4.6×10^{-11} mol cm^{-2} for $[(bpy)(dcb)Ru(bfimbz)Ru(bpy)(dcb^{-})]^{3+}$ and 5.1×10^{-11} mol cm^{-2} for $[(bpy)(dcb)Ru(tpphz)Ru(bpy)(dcb^{-})]^{3+}$, assuming a close-packed surface structure on a relatively flat surface.[18] Thus, the calculated HVSCs are 2.4 and 2.1 for the bfimbz and tpphz systems, respectively. (b) The difference between those values obtained from the absorption ratios and the calculated values could be explained by the fact that, very likely, in perpendicular attachment, the adsorbed molecules may adopt a tilted conformation on the surface (Figure 7a), leading to an increase in vertical surface coverage. It seems reasonable to relate this observation to the limited number of binding sites in $[(bpy)_2Ru(bfimbz)Ru(bpy)(dcb^{2-})]^{2+}$ and $[(bpy)_2Ru(tpphz)Ru(bpy)(dcb^{-})]^{3+}$. These molecules can bind to a TiO_2 surface only through two carboxylic functional groups located on one dcb, allowing the molecule to adjust its spatial conformation, with respect to the surface. However, the rigidity of the BL still prevents bending along the Ru−Ru axis.

(28) Trammell, S. A.; Moss, J. A.; Yang, J. C.; Nakhle, B. M.; Slate, C. A.; Odobel, F.; Sykora, M.; Erickson, B. W.; Meyer, T. J. *Inorg. Chem.* **1999**, *38*, 3665.

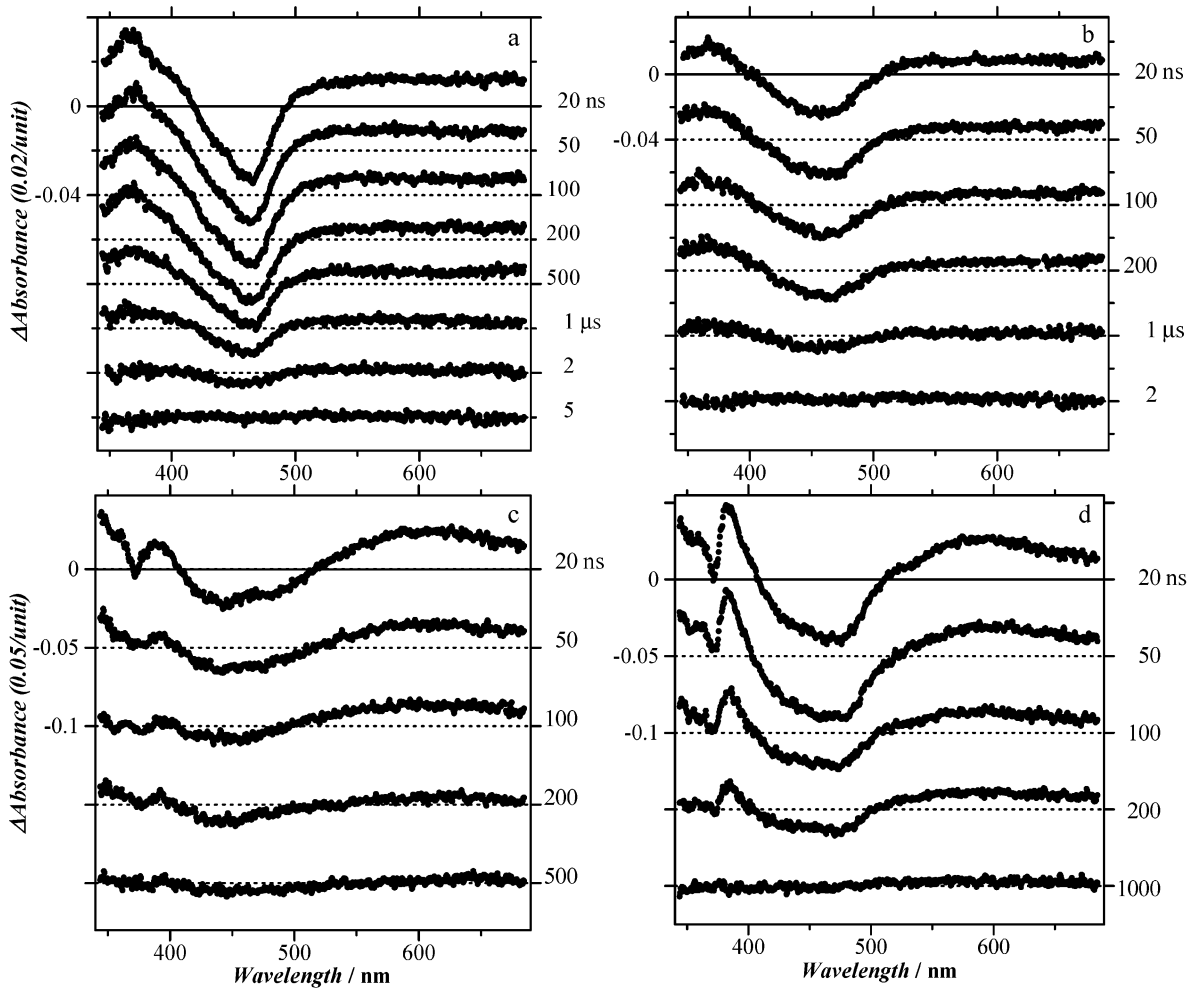

Figure 4. Time-resolved transient absorption spectra (with the corresponding decay rates at 460 nm) of (a) $[(bpy)_2Ru(bfimbz)Ru(bpy)(dcb^{2-})]^{2+}$ (4.2×10^6 and 7.8×10^5 s^{-1}), (b) $[(bpy)(dcb)Ru(bfimbz)Ru(bpy)(dcb^{-})]^{3+}$ (8.5×10^5 s^{-1}), (c) $[(bpy)_2Ru(tpphz)Ru(bpy)(dcb^{-})]^{3+}$ (2.5×10^7 and 1.3×10^6 s^{-1}), and (d) $[(bpy)(dcb)Ru(tpphz)Ru(bpy)(dcb^{-})]^{3+}$ (1.6×10^6 s^{-1}) in argon-saturated MeCN at room temperature ($\lambda_{ex} = 532$ nm).

monolayer composite is formed or not, the surface density of the sensitizer dye is high.

Emission of the binuclear sensitizers upon binding to TiO_2 was strongly quenched, which implies that the MLCT excited state participates in the charge injection process. The weak emissive features, relative to those in solution, were red-shifted by 5−20 nm. The decay of the excited state in argon-saturated MeCN/0.1 M $LiClO_4$ was monitored at 620−650 nm (see Supporting Information, Figure 2s). The decays were fit to triexponential functions including an extremely weak component for which the rate (1.1×10^6 and $\sim 2.0 \times 10^6$ s^{-1} in the bfimbz and tpphz binuclear complexes, respectively) is comparable to that of the sample in neat solvents. The extremely weak component seems to originate from sites electronically uncoupled with the Ti 3d conduction-band manifold.

We could not resolve the fast decay kinetics ($\tau^{-1} > 1 \times 10^9$ s^{-1}) of $[(bpy)_2Ru(bfimbz)Ru(bpy)(dcb^{2-})]^{2+}/TiO_2$ and $[(bpy)(dcb)Ru(bfimbz)Ru(bpy)(dcb^{-})]^{3+}/TiO_2$ with our equipment. However, we were able to measure slower rates (4.8×10^7 and 7.8×10^6 s^{-1}, respectively, in the former and 2.3×10^7 and 4.5×10^6 s^{-1}, respectively, in the latter). These decay kinetics could be explained in terms of quenching of the (Ru → bpy) ^{3}MLCT excited state by intramolecular processes such as (i) electron transfer to the acceptor site of $[Ru^{III}(bpy)(dcb^{m-})]^{n+}/TiO_2(e^-)$ ($m = 1$ or 2 and $n = 2$ or 1) produced during excitation ($\tau < 1$ ns) and (ii) similar to the case in neat solvents, energy transfer to the lower-lying Ru → dcb CT excited state.

On the other hand, we successfully measured rates of 9.5×10^7 s^{-1} in $[(bpy)_2Ru(tpphz)Ru(bpy)(dcb^{-})]^{3+}/TiO_2$ and 5.5×10^7 s^{-1} in $[(bpy)(dcb)Ru(tpphz)Ru(bpy)(dcb^{-})]^{3+}/TiO_2$. We attributed these fast decay kinetics to the quenching of the ^{3}MLCT excited state by interfacial electron transfer from the tpphz radical anion to the Ti 3d conduction-band manifold. The present argument is independently supported by the results of transient absorption spectroscopy (see below). Examples of remote interfacial electron transfer from supramolecular sensitizers can be found in the literature.[4d,e] Those fast rates are followed by slower ones, $(1.5-1.7) \times 10^7$ s^{-1}, which match intercomponent energy transfer rates in $[(bpy)_2Ru(tpphz)Ru(bpy)(dcb^{-})]^{3+}$ in neat solvents.

Transient Absorption Spectra. The transient absorption spectra of dissolved and TiO_2-adsorbed binuclear complexes are depicted in Figures 4 and 5, respectively. In solution, they all show a positive absorption at $\lambda < 400$ nm and a

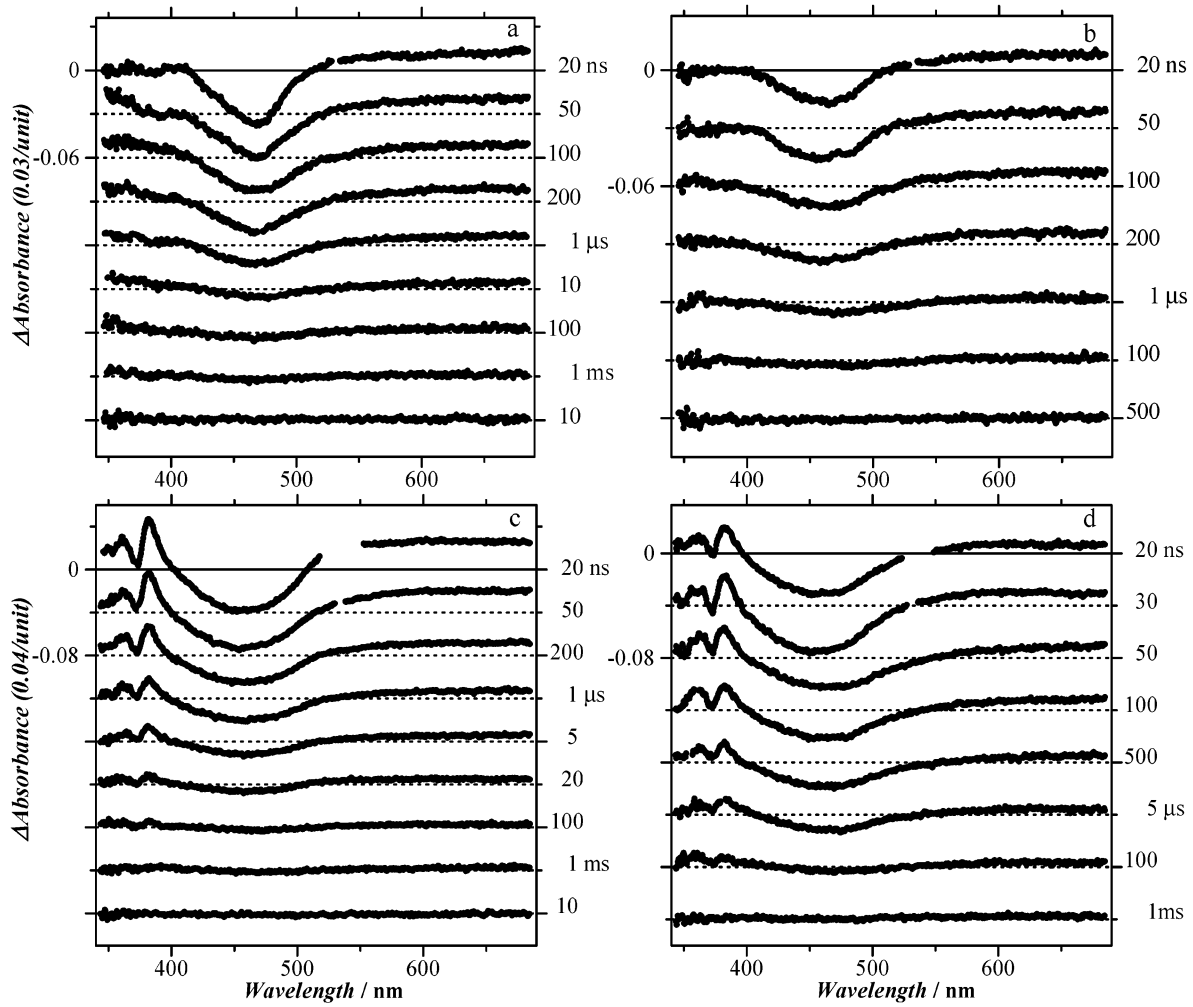

Figure 5. Time-resolved transient absorption spectra (with the corresponding decay rates) of (a) $[(bpy)_2Ru(bfimbz)Ru(bpy)(dcb^{2-})]^{2+}/TiO_2$ (1.7×10^5, 5.3×10^4, and 3.5×10^3 s^{-1} at 460 nm), (b) $[(bpy)(dcb)Ru(bfimbz)Ru(bpy)(dcb^{-})]^{3+}/TiO_2$ (1.2×10^5, 3.1×10^4, and 1.1×10^4 s^{-1} at 380 nm), (c) $[(bpy)_2Ru(tpphz)Ru(bpy)(dcb^{-})]^{3+}/TiO_2$ (3.6×10^5, 4.6×10^4, and 1.4×10^3 s^{-1} at 380 nm; in Supporting Information, Figure 3s), and (d) $[(bpy)(dcb)Ru(tpphz)Ru(bpy)(dcb^{-})]^{3+}/TiO_2$ (5.7×10^5, 5.1×10^4, and 2.7×10^3 s^{-1} at 450 nm) in argon-saturated MeCN containing 0.1 M $LiClO_4$ at room temperature (λ_{ex} = 532 nm).

strong bleaching centered at 460 nm, which is typical of the formation of the ^{3}MLCT excited state of ruthenium(II) polypyridine complexes.[21,29] These features arise following the laser excitation, because of the appearance of transitions within the newly formed polypyridine radical anion and the disappearance of the ground-state MLCT transitions. In the 500−700 nm region, there is clearly a positive weak absorption, which could be attributed to ligand-to-metal charge-transfer transitions that occur between the ligand π-orbital and the dπ-orbital of the transiently formed Ru(III) ion.[29b]

The spectra of the tpphz complexes show additional characteristics at >500 nm, most importantly, a broad positive absorption centered at ca. 580 nm. The pronounced transient absorption in the red spectral region is indicative of a more delocalized ligand radical anion, in this case, $(tpphz)^{\bullet-}$.[8b] Fujita et al. observed a similar transient absorption band with λ_{max} = 550 nm for a free-radical anion generated by pulse radiolysis of phenazine in argon-saturated DMF at room temperature.[30] Amouyal et al. observed the same transient band in the structurally related compound $[(bpy)_2Ru(dppz)]^{2+}$, in which dppz is dipyrido[3,2-*a*:2′,3′-*c*]phenazine.[13] Also, Launay and co-workers extensively investigated the variation in the ground- and excited-state absorption spectra upon addition of $HClO_4$ to MeCN solutions of tpphz complexes.[8b] In these studies, the appearance of the band maximum at longer wavelengths on going from the free-radical anion to the mono- and binuclear complexes could be ascribed to the electron-withdrawing effect of the metal centers, as well as increased π-delocalization in the system.[31]

In the excited state, the intraligand $\pi-\pi^*$ transitions of tpphz were shifted to lower energies, because of the electrostatic effect of the highly charged metal ion, i.e., the already formed Ru(III) core. These new bands appeared at

(29) (a) Braterman, P. S.; Harriman, A.; Heath, G. A.; Yellowless, L. *J. Chem. Soc., Dalton Trans.* **1983**, 1801. (b) Gholamkhass, B.; Nozaki, K.; Ohno, T. *J. Phys. Chem. B* **1997**, *101*, 9010.

(30) Fujita, M.; Ishida, A.; Majima, T.; Takamuku, S. *J. Phys. Chem.* **1996**, *100*, 5382.

(31) Gholamkhass, B. Ph.D. Dissertation, Osaka University, Osaka, Japan, 1998.

360 and 390 nm in $[(bpy)_2Ru(tpphz)Ru(bpy)(dcb^-)]^{3+}$ and at 360 and 385 nm in $[(bpy)(dcb)Ru(tpphz)Ru(bpy)(dcb^-)]^{3+}$.[32] Accordingly, the 370-nm ground-state $\pi-\pi^*$ transition was bleached, whereas depletion of the other band at 350 nm was obscured by the strong positive absorption in this region, which is mainly composed of $\pi-\pi^*$ transitions in bpy-type anion radicals.[8,20,21,29] All the transients decay with the same kinetics and lifetimes as those observed for the corresponding emissions. The decay rates are given in the caption of Figure 4.

The transient absorption spectra of the TiO_2-adsorbed samples (Figure 5) are clearly different from those in solution (Figure 4). The initial spectra resemble, but are not identical to, those of MLCT excited states. The recovery of the ground-state spectrum due to charge recombination occurs on a time scale of several hundred microseconds to milliseconds (Figure 5), which indicates that recapture of the conduction band electron by the oxidized Ru center is a relatively slow process. The prolonged lifetime of the charge-separated state is most likely a consequence of the long distance between the TiO_2 surface and the hole on the remote Ru(III) core.

In bfimbz complexes, the MLCT band bleaches, as expected. However, the spectra lack the polypyridine radical anion absorption at $\lambda < 400$ nm. The absence of positive absorption at $\lambda < 400$ nm in bfimbz compounds indicates that electron injection (for example, in the case of $[(bpy)_2Ru_A(bfimbz)Ru_B(bpy)(dcb^{2-})]^{2+}$) occurs very fast.

$$h\nu + Ru_A(II)-Ru_B(II)-TiO_2 \rightarrow Ru_A(II)-{}^*Ru_B(II)-TiO_2 \quad (2a)$$

$$h\nu + Ru_A(II)-Ru_B(II)-TiO_2 \rightarrow {}^*Ru_A(II)-Ru_B(II)-TiO_2 \quad (2b)$$

$${}^*Ru_A(II)-Ru_B(II)-TiO_2 \rightarrow Ru_A(II)-{}^*Ru_B(II)-TiO_2 \quad (2c)$$

Therefore, all the excited $^*Ru_B(II)$ produced via direct excitation (eq 2a) and/or intercomponent energy transfer (eq 2c) has participated in the electron injection process (eq 3) within the excitation time scale (10 ns).

$$Ru_A(II)-{}^*Ru_B(II)-TiO_2 \rightarrow Ru_A(II)-Ru_B(III)-TiO_2(e^-) \quad (3)$$

The transient absorption spectra of the tpphz complexes (Figure 5c and d) are very informative. Close inspection of Figure 5c, for example, reveals the appearance of two sharp bands, at 361 and 382 nm, associated with intraligand $\pi-\pi^*$ transitions in Ru(III)-coordinated tpphz. Particularly at $\lambda >$ 370 nm, the transient spectra superimpose to a simulated spectrum for the formation of $[(bpy)_2Ru^{III}(tpphz)Ru^{II}(bpy)_2]^{5+}$ from the ground state, with the electron being transferred to the conduction band of TiO_2 (there is a certain amount of the excited state in each case[33]). This is convincingly illustrated in Figure 6, which shows the early-time transient spectra of TiO_2-adsorbed $[(bpy)_2Ru(tpphz)Ru(bpy)(dcb^-)]^{3+}$ and $[(bpy)(dcb)Ru(tpphz)Ru(bpy)(dcb^-)]^{3+}$, together with the simulated spectra. Deviations at shorter wavelengths ($\lambda <$ 370 nm) could be ascribed to an overestimation in the absorption spectrum of the 5+ species.

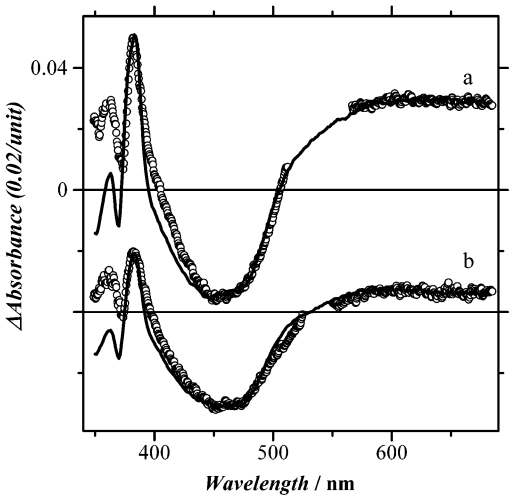

Figure 6. Simulated transient absorption spectra for the electron injection products of (a) $[(bpy)_2Ru(tpphz)Ru(bpy)(dcb^-)]^{n+}/TiO_2(e^-)$ and (b) $[(bpy)(dcb)Ru(tpphz)Ru(bpy)(dcb^-)]^{n+}/TiO_2(e^-)$. The ground-state spectra in MeCN were subtracted from the absorption spectrum of $[(bpy)_2Ru(tpphz)Ru(bpy)_2]^{5+}$ in MeCN/0.1 M TBAH and added to the difference-absorption spectrum of a bare $TiO_2(e^-)$ reported in ref 34. The resulting spectra (solid lines) include 20% and 50% of the excited-state transient spectra measured at 20 ns following the excitation of $[(bpy)_2Ru(tpphz)Ru(bpy)(dcb^-)]^{3+}$ and $[(bpy)(dcb)Ru(tpphz)Ru(bpy)(dcb^-)]^{3+}$ in MeCN, respectively. The open circles in parts a and b are the experimental spectra observed at 20 ns (panels c and d of Figure 5, respectively). See text for details.

In the early-time transient spectra of TiO_2-adsorbed $[(bpy)(dcb)Ru(tpphz)Ru(bpy)(dcb^-)]^{3+}$, the tpphz radical anion absorption is observable during and shortly after the excitation (20−30 ns in Figure 5d). The longer wavelength flat absorbance, which is attributed to intraband transitions or free charge-carrier absorption, is reminiscent of electron injection into TiO_2.[34] Furthermore, a noticeable increase in the intensity of the 361- and 382-nm peaks and the longer wavelength band ($\lambda >$ 550 nm), as well as the 450 nm bleaching at 30 ns (compared to those at 20 ns), reveals that, in this heterotriad, transition from the ^{3}MLCT excited state to a charge-separated one, i.e., the electron injection, is a slow process. In the case of $[(bpy)_2Ru(tpphz)Ru(bpy)(dcb^-)]^{3+}/TiO_2$, such a slow process cannot be resolved,

(32) For the same reason, upon one-electron oxidation of one of the metal sites in $[(bpy)_2Ru(tpphz)Ru(bpy)_2]^{4+}$, peaks at 350 and 370 nm were shifted to 363 and 383 nm, respectively. Details are reported in ref 31.

(33) In practice, the ground-state absorption spectra of $[(bpy)_2Ru(tpphz)Ru(bpy)(dcb^-)]^{3+}$ and $[(bpy)(dcb)Ru(tpphz)Ru(bpy)(dcb^-)]^{3+}$ in MeCN were subtracted from the absorption spectrum of electrochemically generated $[(bpy)_2Ru(tpphz)Ru(bpy)_2]^{5+}$ in MeCN/0.1 M TBAH (see refs 29b and 31 for details). The new spectra were then added to a difference-absorption spectrum of a bare TiO_2 electrode in aqueous 0.2 M $LiClO_4$ measured at −1000 and +1000 mV ($\epsilon = 3400\ M^{-1}\ cm^{-1}$ at 780 nm).[34] The resulting spectra were mixed with 20% and 50% of the excited-state transient spectra measured at 20 ns following the excitation of $[(bpy)_2Ru(tpphz)Ru(bpy)(dcb^-)]^{3+}$ and $[(bpy)(dcb)Ru(tpphz)Ru(bpy)(dcb^-)]^{3+}$ in MeCN, respectively. The difference molar absorption coefficients of the ^{3}MLCT excited state of the binuclear complexes were obtained by assuming 100%-efficient energy transfer to anthracene. Details are reported in: Ohno, T.; Yoshimura, A.; Mataga, N. *J. Phys. Chem.* **1990**, *94*, 4871.

(34) Rothenberger, G.; Fitzmaurice, D.; Grätzel, M. *J. Phys. Chem.* **1992**, *96*, 5983.

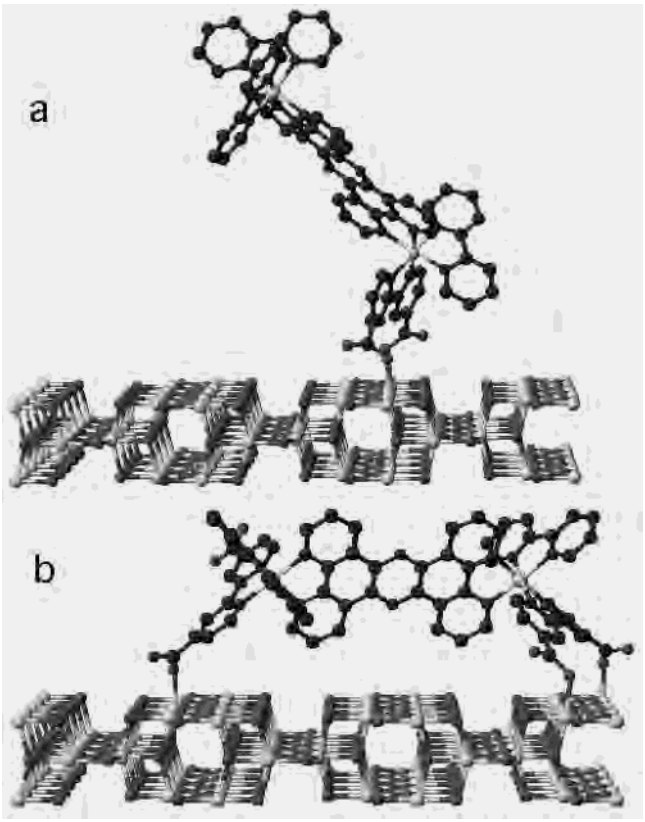

Figure 7. Illustrations of the geometric features of the deposited dye molecules (a) $[(bpy)_2Ru(tpphz)Ru(bpy)(dcb^-)]^{3+}/TiO_2$ and (b) $[(bpy)(dcb)Ru(tpphz)Ru(bpy)(dcb^-)]^{3+}/TiO_2$ on an infinite lattice of anatase crystal. The illustrations were generated with the CAChe 3D-stereo molecule-building application. See text for details.

because of the shorter lifetime of its ^{3}MLCT excited state (estimated lifetime is ca. 10 ns from the emission data).

To understand the reason behind the observation of different electron injection rates in TiO_2-adsorbed $[(bpy)_2Ru(tpphz)Ru(bpy)(dcb^-)]^{3+}$ and $[(bpy)(dcb)Ru(tpphz)Ru(bpy)(dcb^-)]^{3+}$, we used the CAChe 3D-stereo molecule-building application to determine the geometric features of the deposited dye. We first built an infinite anatase crystal lattice[35] and then locked the positions of all the O and Ti atoms in the anatase block. We separately created the molecular structures of the binuclear compounds and used the MM2 force field to generate the minimum-energy conformations. Dye molecules were *deposited* on the surface by creating *ester bonds* (two for heterobinuclear complexes and three for homobinuclear complexes) between surface Ti atoms and carboxylic O atoms.[36] To assess the geometric features, we once again generated the minimum-energy conformation for the deposited molecules. Figure 7 shows views of $[(bpy)_2Ru(tpphz)Ru(bpy)(dcb^-)]^{3+}$ and $[(bpy)(dcb)Ru(tpphz)Ru(bpy)(dcb^-)]^{3+}$ on the anatase surfaces. In the former (Figure 7a), the geometry optimization led to a dihedral angle of 42° and a shortest $N_{phenazine}-Ti_{surface}$ distance of 12.5 Å. In the latter (Figure 7b), those parameters are 70° and 5.5 Å, respectively, and, despite the shorter donor−acceptor distance, the electron injection rate (assumed to be the same as emission decay of 5.5×10^7 s^{-1}, versus 9.5×10^7 s^{-1}) is smaller by a factor of 2. It seems that, in addition to the donor−acceptor distance, the injection rate is remarkably dependent upon donor orbital orientation. We conclude that, indeed, the electron injection is associated with transfer from the tpphz π^*-orbital that is nominally orthogonal to the CT axis in the $[(bpy)(dcb)Ru(tpphz)Ru(bpy)(dcb^-)]^{3+}/TiO_2$ system. In the heterobinuclear complex, the tpphz π^*-orbital faces the semiconductor surface, which allows better electronic communication across the CT axis.[27b]

In the $[(bpy)_2Ru^{II}(bfimbz)Ru^{III}(bpy)(dcb)]^{n+}/TiO_2(e^-)$ system, the positive absorption at $\lambda < 400$ nm appears in the transient spectra when $\tau > 50$ ns (Figure 5a). With the exception of the flat absorption at longer wavelengths, the transient spectrum at, for example, 100 ns resembles that of the MLCT excited state in neat solvent, which implies the presence of an excited state of the electron injection product, $[(bpy)_2*Ru(bfimbz)Ru^{III}(bpy)(dcb)]^{n+}/TiO_2(e^-)$ (eq 4), and/or the electron (hole) transfer product, $[(bpy)_2Ru^{III}(bfimbz)Ru^{II}(bpy)(dcb)]^{n+}/TiO_2(e^-)$ (eq 5), both with presumably similar spectral features within the observation window ($\lambda > 340$ nm).[37]

$$h\nu + Ru_A(II)-Ru_B(III)-TiO_2(e^-) \rightarrow {}^*Ru_A(II)-Ru_B(III)-TiO_2(e^-) \quad (4)$$

$$Ru_A(II)-Ru_B(III)-TiO_2(e^-) \rightarrow Ru_A(III)-Ru_B(II)-TiO_2(e^-) \quad (5)$$

However, an estimated delay of 25 ns in the production of this state can only be explained by the occurrence of an intramolecular electron transfer (eq 5) to produce $[(bpy)_2Ru^{III}(bfimbz)Ru^{II}(bpy)(dcb)]^{n+}/TiO_2(e^-)$, placed 0.04 eV[38] above the initial electron-injection product $[(bpy)_2Ru^{II}(bfimbz)Ru^{III}(bpy)(dcb)]^{n+}/TiO_2(e^-)$.[39] Such a mechanism (eq 5) seems less likely for $[(bpy)_2Ru(tpphz)Ru(bpy)(dcb^-)]^{3+}/TiO_2$. However, production of the electron-transfer product $[(bpy)_2Ru^{III}(tpphz)Ru^{II}(bpy)(dcb)]^{n+}/TiO_2(e^-)$ from the higher excited state of $[(bpy)_2*Ru(tpphz)Ru^{III}(bpy)(dcb)]^{n+}/TiO_2(e^-)$ or as

(35) The anatase crystal block was built using fractional coordinates of the asymmetric atoms, a tetragonal space group symmetry of $I4_1/amd$ ($a = b = 3.7852$ Å, $c = 9.5139$ Å, $\alpha = \beta = \gamma = 90°$), and lattice boundaries of 4, 1, and 3 in the *a*-, *b*-, and *c*-directions, respectively.

(36) For homobinuclear complexes, deposition of the dye molecule on the surface through four ester bonds has led to deformation of the bpy planar structure. Therefore, only three ester bonds were formed to deposit the molecule.

(37) Remarkable differences in the spectral features of $[(bpy)_2*Ru(BL_1)Ru^{III}(bpy)(dcb)]^{n+}/TiO_2(e^-)$ and $[(bpy)_2Ru^{III}(BL_1)Ru^{II}(bpy)(dcb)]^{n+}/TiO_2(e^-)$, where BL_1 = bfimbz, are expected at shorter wavelengths ($\lambda < 400$ nm), because of the presence of either a bpy-type radical anion ($\lambda_{max} = 370$ nm, reported for $[*Ru(bpy)_3]^{2+}$),[13] in the former, or Ru(III)-coordinated bpy absorptions (which is basically the same as those of Ru(II) compounds),[29b] in both the former and latter. Close examination of transient spectra in Figure 5a shows that the absorption band at $\lambda < 400$ nm peaks well below 370 nm.

(38) The approximate energies are estimated on the basis of electrochemical measurements in solution.

(39) The rise time for this state was determined to be 25 ns, from the analysis of the transient absorption change at 360 nm. We point out that, even if the observed features are due to the $[(bpy)_2*Ru(bfimbz)Ru^{III}(bpy)(dcb^{2-})]^{n+}/TiO_2(e^-)$ excited state (which can be prepared within the laser excitation (10 ns), because of an ultrafast electron injection from the vicinal Ru to TiO_2[41]), its main deactivation pathway is an oxidative quenching to give the electronic isomer $[(bpy)_2Ru^{III}(bfimbz)Ru^{II}(bpy)(dcb^{2-})]^{n+}/TiO_2(e^-)$.

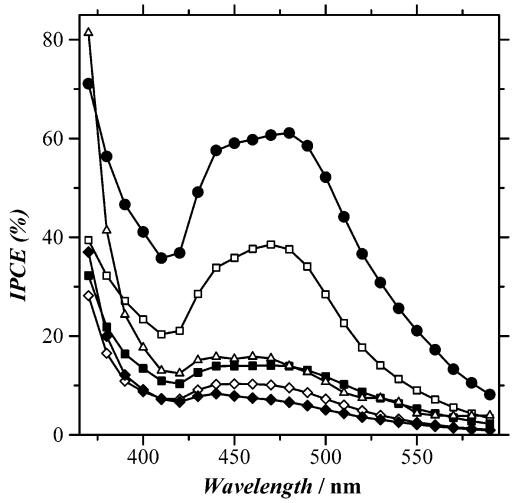

Figure 8. Plot of incident photon-to-current conversion efficiency (IPCE), as a function of excitation wavelength, λ, calculated from the expression $1240I_p/\lambda F$, where I_p is the photocurrent density (given in μA/cm^2) and F is the photon flux (given in μW/cm^2). Legend is as follows: (●) $[(bpy)Ru(dcb)_2]^{2+}/TiO_2$, (□) $[(bpy)_2Ru(bfimbz)Ru(bpy)(dcb^{2-})]^{2+}/TiO_2$, (△) $[(bpy)_2Ru(bfimbz)Ru(dcb)(dcb^{2-})]^{2+}/TiO_2$, (◇) $[(bpy)(dcb)Ru(bfimbz)Ru(bpy)(dcb^{-})]^{3+}/TiO_2$, (■) $[(bpy)_2Ru(tpphz)Ru(bpy)(dcb^{-})]^{3+}/TiO_2$, and (◆) $[(bpy)(dcb)Ru(tpphz)Ru(bpy)(dcb^{-})]^{3+}/TiO_2$ (all in argon-purged MeCN containing 0.1 M KI and 0.05 M I_2). IPCEs are relative to the value of $[Ru(dcb)_2(H_2O)_2]^{2-}/TiO_2$ reported in: Liska, P.; Vlachopoulos, N.; Nazeeruddin, M. K.; Comte, P.; Grätzel, M. *J. Am. Chem. Soc*. **1988**, *110*, 3686.

a result of direct electron injection from excited $*Ru_A(II)$ cannot be ruled out. Evidences for the occurrence of an efficient and direct electron injection from remote chromophoric sites have been reported in the literature.[4d,40]

Photovoltaic Feature. Photocurrent measurements were performed on the TiO_2 electrodes sensitized with the ruthenium complexes. The corresponding photoaction spectra (Figure 8) show that, in this series of sensitizers, the highest incident monochromatic photon-to-current conversion efficiency (IPCE) was obtained with $[(bpy)_2Ru(bfimbz)Ru(bpy)(dcb^{2-})]^{2+}/TiO_2$ (39% at 470 nm). In this structurally rigid binuclear sensitizer, the multiexponential charge recombination rate falls in the micro- to millisecond time range. Therefore, the higher value of IPCE in this heterotriad system could be interpreted in terms of (i) a fast electron injection initiated from a dcb-localized MLCT and (ii) an improved molecular orientation on the surface, because of rigidity and, at the same time, linearity of the heterotriad system, resulting in a slower charge recombination between the injected electron and the hole presumably on the remote Ru(III) core. On the other hand, the photocurrent efficiency of the homobinuclear complexes, where both metallic moieties are bound to the surface, is rather low, because of the absence of a remote hole scavenger.

Comparison of the IPCE values of the homo- and heterobinuclear complexes shows that the efficiencies are lower in the tpphz complexes. The main reason could be the slower rate of the remote electron injection, from a BL (tpphz) localized excited state, and its competition with the other excited-state decay processes. Considering the fact that electron injection originates from the tpphz π^*-orbital, the electron must traverse the through-space pathway from the donor π^*-orbital to the acceptor Ti 3d conduction-band manifold, which results in an inefficient interfacial electron transfer. Further decrease in the efficiency of the tpphz homobinuclear complex (7% at 460 nm) can be explained by the geometric features of the deposited dye; the tpphz π^*-orbital is orthogonal to the CT axis, thus lacking sufficient electronic communication in the $[(bpy)(dcb)Ru(tpphz)Ru(bpy)(dcb^{-})]^{3+}/TiO_2$ system.

Inefficient conversions in $[(bpy)_2Ru(tpphz)Ru(bpy)(dcb^{-})]^{3+}/TiO_2$ (14% at 470 nm) and $[(bpy)_2Ru(bfimbz)Ru(dcb)(dcb^{2-})]^{2+}/TiO_2$ (16% at 460 nm) could be related to the inaccessibility of the electronic isomer states of $[(bpy)_2Ru^{III}(tpphz)Ru^{II}(bpy)(dcb)]^{n+}/TiO_2(e^-)$ and $[(bpy)_2Ru^{III}(bfimbz)Ru^{II}(dcb)_2]^{n+}/TiO_2(e^-)$, placed 0.09 and 0.25 eV[37] above the initial interfacial electron-transfer products $[(bpy)_2Ru^{II}(tpphz)Ru^{III}(bpy)(dcb)]^{n+}/TiO_2(e^-)$ and $[(bpy)_2Ru^{II}(bfimbz)Ru^{III}(dcb)_2]^{n+}/TiO_2(e^-)$, respectively.

Conclusions

We have described the covalent assembly of an anatase TiO_2 nanocrystal and ruthenium binuclear complexes to form a heterotriad system capable of performing useful tasks such as solar energy conversion. We have shown that visible excitation of the heterotriad assemblies at a wavelength of 532 nm resulted in formation of the ^{3}MLCT excited state of the ruthenium binuclear sensitizer, $Ru(BL)Ru/TiO_2$, where BL = tetrapyrido[3,2-*a*:2′,3′-*c*:3″,2″-*h*:2‴,3‴-*j*]phenazine (tpphz), and succeeding electron injection. We did not detect an excited-state spectrum for the BL = 1,4-bis([1,10]-phenanthroline[5,6-*d*]imidazol-2-yl)benzene (bfimbz) complexes, because of an ultrafast electron injection, initiated from a dcb-localized MLCT to the Ti 3d conduction band.[41] In the tpphz heterotriad assemblies, the electron injection from a remote tpphz site was remarkably dependent on donor orbital orientation. In particular, in the $[(bpy)(dcb)Ru(tpphz)Ru(bpy)(dcb^{-})]^{3+}/TiO_2$ system, the tpphz π^*-orbital is orthogonal to the charge-transfer axis, and this plays a key role in defining the donor−acceptor electronic communication.

The findings reported in this study establish that, in the heterotriad assembly, the slow rate of charge recombination is a direct result of an improved molecular orientation on the surface, because of rigidity of the heterotriad system. According to electrochemical data, part of the converted energy is consumed as the driving force for the uphill electron transfer, which results in photocurrent efficiencies lower than those of sensitizers commonly used in regenerative solar cells.[1] However, an understanding of the interfacial and intramolecular electron-transfer mechanisms observed in these assemblies opens the door to utilizing such reactions for photon harvesting and electron transfer to redox-active trap sites.

(40) Lees, A. C.; Kleverlaan, C. J.; Bignozzi, C. A.; Vos, J. G. *Inorg. Chem.* **2001**, *40*, 5343.

(41) Tachibana, Y.; Moser, J. E.; Grätzel, M.; Klug, D. R.; Durrant, J. R. *J. Phys. Chem*. **1996**, *100*, 20056.

Acknowledgment. We thank the Japanese Ministry of Economy, Trade and Industry for financial support. B.G. gratefully acknowledges the Japan Science and Technology Corporation (JST) for a research fellowship.

Supporting Information Available: Selected proton NMR spectra of $[(bpy)_2Ru(fimbzl)](PF_6)_2$ and $[(bpy)_2Ru(tpphz)Ru(bpy)(dcb^-)](PF_6)_3$, emission decay kinetics of $[(bpy)_2Ru(tpphz)Ru(bpy)(dcb^-)]^{3+}/TiO_2$ and $[(bpy)(dcb)Ru(tpphz)Ru(bpy)(dcb^-)]^{3+}/TiO_2$, and transient-absorption decay profile of $[(bpy)_2Ru(tpphz)Ru(bpy)(dcb^-)]^{3+}/TiO_2$ in argon-saturated MeCN containing 0.1 M $LiClO_4$. This material is available free of charge via the Internet at http://pubs.acs.org.

IC0341237